Heavy quark spin multiplet structure of P_c-like pentaquarks as a P-wave hadronic molecular state

Yuki Shimizu[1,*], Yasuhiro Yamaguchi[2], and Masayasu Harada[1]

[1]*Department of Physics, Nagoya University, Nagoya 464-8602, Japan*
[2]*Theoretical Research Division, Nishina Center, RIKEN, Hirosawa, Wako, Saitama 351-0198, Japan*
*E-mail: yshimizu@hken.phys.nagoya-u.ac.jp

....
We study the heavy quark spin (HQS) multiplet structure of P-wave $Q\bar{Q}qqq$-type pentaquarks treated as molecules of a heavy meson and a heavy baryon. We define the light-cloud spin (LCS) basis decomposing the meson–baryon spin wave function into LCS and HQS parts. Introducing the LCS basis, we find HQS multiplets classified by the LCS: five HQS singlets, two HQS doublets, and three HQS triplets. We construct the one-pion exchange potential respecting the heavy quark spin and chiral symmetries to demonstrate which HQS multiplets are realized as a bound state. By solving the coupled channel Schrödinger equations, we study the heavy meson–baryon systems with $I = 1/2$ and $J^P = (1/2^+, 3/2^+, 5/2^+, 7/2^+)$. The bound states which have the same LCS structure are degenerate at the heavy quark limit, and the degeneracy is resolved for finite mass. This HQS multiplet structure will be measured in future experiments.
....
Subject Index   D32

1. Introduction

In 2015, the Large Hadron Collider beauty experiment (LHCb) Collaboration observed two hidden charm pentaquarks, $P_c^+(4380)$ and $P_c^+(4450)$ [1–3]. Their masses are $M_{P_c(4380)} = 4380 \pm 8 \pm 28$ MeV and $M_{P_c(4450)} = 4449.8 \pm 1.7 \pm 2.5$ MeV, and their decay widths are $\Gamma_{P_c(4380)} = 205 \pm 18 \pm 86$ MeV and $\Gamma_{P_c(4450)} = 39 \pm 5 \pm 19$ MeV. Their spin and parity are not determined. One state has $J = 3/2$ and the other has $J = 5/2$, and their parity is opposite.

The P_c pentaquarks have a charm quark and an anti-charm quark. They are called the hidden-charm pentaquarks. There were some theoretical works on hidden-charm pentaquarks before the LHCb announcement [4–7]. After the LHCb observation, many theoretical studies have been conducted in various ways: the hadronic molecular picture [8–24], quark model estimation [25–27], the diquark picture [28–32], the quark-cluster model [33], the baryocharmonium model [34], the hadroquarkonia model [35], the soliton model [36], holographic QCD [37], and the hadronic molecule coupled with a five-quark state [38]. Some review papers have also been published [39–41].

The hadronic molecular picture is one highly possible model around the hadron threshold. The threshold of $\bar{D}\Sigma_c^*$ is 4385.3 MeV and that of $\bar{D}^*\Sigma_c$ is 4462.2 MeV. These values are slightly above the masses of $P_c(4380)$ and $P_c(4450)$, respectively. Therefore, the P_c pentaquarks are candidates for the loosely bound state of a charmed meson and a charmed baryon.

Recently, the LHCb Collaboration reported a new result for the P_c pentaquarks [42]. Their masses and widths are

$$P_c(4312): \quad M = 4311.9 \pm 0.7^{+6.8}_{-0.6} \, \text{MeV},$$

$$\Gamma = 9.8 \pm 2.7^{+3.7}_{-4.5} \, \text{MeV},$$

$$P_c(4440): \quad M = 4440.3 \pm 1.3^{+4.1}_{-4.7} \, \text{MeV},$$

$$\Gamma = 20.6 \pm 4.9^{+8.7}_{-10.1} \, \text{MeV},$$

$$P_c(4457): \quad M = 4457.3 \pm 0.6^{+4.1}_{-1.7} \, \text{MeV},$$

$$\Gamma = 6.4 \pm 2.0^{+5.7}_{-1.9} \, \text{MeV}.$$

A narrow peak of the $P_c(4450)$ splits into two peaks, $P_c(4440)$ and $P_c(4457)$, which are close to the $\bar{D}^* \Sigma_c$ threshold. Moreover, the mass of $P_c(4312)$ is just below the threshold of the $\bar{D}\Sigma_c$. This new experimental result motivated further theoretical analysis [43–52]. Although the spin and parity were not measured in the experiment, many theoretical studies suggest that these P_c pentaquarks are the negative parity state.

In the heavy quark effective theory, the spin-dependent interaction of a heavy quark is suppressed by the inverse of the heavy quark mass, $1/m_Q$. At the heavy quark limit, therefore, the dynamics is independent of the transformation of the heavy quark spin. This is called heavy quark spin symmetry (HQSS). The suppression of the spin-dependent force causes decomposition of the heavy quark spin and the light-cloud spin at the heavy quark limit [53–57]:

$$\vec{J} = \vec{s}_{\text{light}} + \vec{s}_{\text{heavy}}. \tag{1}$$

The total angular momentum $\vec{J}$ is a conserved quantity, and the heavy quark spin $\vec{s}_{\text{heavy}}$ is conserved at the heavy quark limit. Thus, the light-cloud spin $\vec{s}_{\text{light}}$ is also conserved.

HQSS leads to mass degeneracy between the heavy hadrons with different spin. Considering a heavy meson $P^{(*)} \sim Q\bar{q}$ with a heavy quark Q and an anti-light quark $\bar{q}$, the total spin of $Q\bar{q}$ is

$$J_\pm = 1/2 \pm 1/2, \tag{2}$$

and $J_+ = 1$ ($J_- = 0$) for the vector meson P^* (the pseudoscalar meson P), because of the quark spin $1/2$. Their difference comes from the spin configuration of the light-cloud and heavy quark spins. However, the system is independent of the heavy quark spin, and as a result the spin 0 state P and the spin 1 state P^* degenerate at the heavy quark limit. This structure is called the HQS doublet.

In the real world, however, the quark masses are finite, so that there exists a mass difference between the pseudoscalar and vector mesons. For example, the mass difference between the pseudoscalar meson K and the vector meson K^* is about 400 MeV. By contrast, the mass splitting between D and D^* is about 140 MeV and between B and B^* is 45 MeV. The mass difference is much smaller in the charm and bottom quark sectors than in the light quark sector. There is the same tendency in the single heavy baryon. The mass difference between the spin 1/2 baryon Σ_c and spin 3/2 baryon Σ_c^* is about 65 MeV, and between Σ_b and Σ_b^* is about 20 MeV.

The purpose of this work is to apply HQSS to $Q\bar{Q}qqq$-type pentaquarks as hadronic molecular states of a $\bar{P}^{(*)}$ meson and a $\Sigma_Q^{(*)}$ baryon. Here, $\bar{P}$ and $\bar{P}^*$ denote mesons with $J^P = 0^-$ and 1^- with an anti-heavy quark, like $\bar{D}$ and $\bar{D}^*$ mesons, and Σ_Q and Σ_Q^* the baryons with $J^P = 1/2^+$ and $3/2^+$ with a heavy quark, like Σ_c and Σ_c^* baryons. We note that the HQS doublet structure of
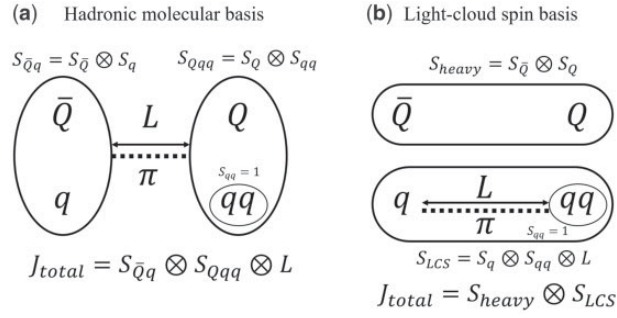
Fig. 1. Schematic pictures of the heavy meson–heavy baryon molecular basis (left panel) and light-cloud spin basis (right panel). The circles mean the combination of spins. They do not imply the quark component in a hadron. Therefore, the $\bar{Q}Q$ and the qqq are not a quarkonium and a nucleon. S_α is the spin of α and L is the orbital angular momentum. The orbital angular momentum is carried between a light quark and a light diquark in the light cloud.

single heavy hadrons such as $\bar{P}^{(*)}$ and $\Sigma_Q^{(*)}$ is well known. Furthermore, the HQS multiplet structure of a multi-hadron system with a single heavy quark like $\bar{P}^{(*)}N$ molecular states has been studied in Refs. [58–60]. On the other hand, the doubly heavy system does not strictly have HQSS. It is interesting to apply HQSS to doubly heavy pentaquarks under the assumption that the two heavy quarks are labeled by the same velocity. In this paper we study the consequences of HQSS in the $\bar{P}^{(*)}\Sigma_Q^{(*)}$ molecular states.

To deal with the HQSS of the $\bar{P}^{(*)}\Sigma_Q^{(*)}$ molecular states, we define the light-cloud spin (LCS) basis, which is more suitable than the hadronic molecular (HM) basis. The HM basis is given by the coupling of spins $S_{\bar{Q}q}$ for a $\bar{Q}q$ meson and S_{Qqq} for a Qqq baryon, and the relative orbital angular momentum L between a heavy meson and a baryon, which is written as $[L[[S_{\bar{Q}}S_q]_{S_{\bar{Q}q}}[S_QS_{qq}]_{S_{Qqq}}]_S]_{J_{total}}$, as shown in Fig. 1(a). S_Q ($S_{\bar{Q}}$) is the heavy quark (antiquark) spin, S_q (S_{qq}) is the light quark (diquark) spin, and J_{total} is the total angular momentum. The LCS basis is obtained by rearranging the spin of the HM basis, and then these bases are transferred by the unitary transformation of each other. The LCS basis is given by the coupling of the heavy quark spin $S_{heavy} = S_{\bar{Q}} \otimes S_Q$ and the light-cloud spin $S_{LCS} = S_q \otimes S_{qq} \otimes L$, where the heavy and light cloud spins are decomposed as in Eq. (1). This basis is expressed by $[[S_{\bar{Q}}S_Q]_{S_{heavy}}[L[S_qS_{qq}]_{S_{qqq}}]_{S_{LCS}}]_{J_{total}}$, as shown in Fig. 1(b). We note that the circles surrounding $\bar{Q}q$, Qqq, etc. in Fig. 1 represent the set of (di)quark spins such as $[S_{\bar{Q}}S_q]$ and $[S_{\bar{Q}}S_Q]$, while it does not mean the color singlet hadron. For instance, the set of $\bar{Q}Q$ (qqq) in the LCS basis represents the coupled spin $S_{\bar{Q}Q}$ (S_{qqq}), but does not mean the quarkonium (nucleon). The object $\bar{Q}Q$ (qqq) can be the color octet state as long as the whole system $\bar{Q}Qqqq$ is the color singlet one.

The relative motion between two heavy quarks cannot be neglected even for the lowest order, as discussed in the heavy quarkonium effective theory [75–77]. In particular, the internal motion is needed to include the orbital angular momentum excitation for the heavy quarkonium. In this study, however, we assume that both the heavy quark and anti-heavy quark are at rest. Instead, the orbital angular momentum is carried by an interaction between a light quark in a heavy meson and a light diquark in a heavy baryon. It then seems that a heavy quark is surrounded by the light degree of freedom, so we named this picture the light-cloud spin basis. We discuss the structure of the HQS multiplet under the assumption that HQSS is (approximately) established by the model of the LCS basis.

Table 1. Possible spin states of the P-wave $\bar{P}^{(*)}\Sigma_Q^{(*)}$ molecular states for given J^P. $\left(^{2S+1}L_J\right)$ denotes the total spin of meson and baryon S, the orbital angular momentum L, and the total angular momentum J.

J^P	
$\frac{1}{2}^+$	$\bar{P}\Sigma_Q\left(^2P_{1/2}\right), \bar{P}\Sigma_Q^*\left(^4P_{1/2}\right), \bar{P}^*\Sigma_Q\left(^2P_{1/2}\right), \bar{P}^*\Sigma_Q\left(^4P_{1/2}\right), \bar{P}^*\Sigma_Q^*\left(^2P_{1/2}\right),$ $\bar{P}^*\Sigma_Q^*\left(^4P_{1/2}\right)$
$\frac{3}{2}^+$	$\bar{P}\Sigma_Q\left(^2P_{3/2}\right), \bar{P}\Sigma_Q^*\left(^4P_{3/2}\right), \bar{P}^*\Sigma_Q\left(^2P_{3/2}\right), \bar{P}^*\Sigma_Q\left(^4P_{3/2}\right), \bar{P}^*\Sigma_Q^*\left(^2P_{3/2}\right),$ $\bar{P}^*\Sigma_Q^*\left(^4P_{3/2}\right), \bar{P}^*\Sigma_Q^*\left(^6P_{3/2}\right)$
$\frac{5}{2}^+$	$\bar{P}\Sigma_Q^*\left(^4P_{5/2}\right), \bar{P}^*\Sigma_Q\left(^4P_{5/2}\right), \bar{P}^*\Sigma_Q^*\left(^4P_{5/2}\right), \bar{P}^*\Sigma_Q^*\left(^6P_{5/2}\right)$
$\frac{7}{2}^+$	$\bar{P}^*\Sigma_Q^*\left(^6P_{7/2}\right)$

The HQS multiplet structure of $\bar{P}^{(*)}\Sigma_Q^{(*)}$ with S-wave has been studied in Ref. [61]. The analysis of the S-wave state covers the negative parity pentaquarks. After the recent LHCb result [42], we discussed the HQS multiplet structure of the observed pentaquarks based on the LCS basis [46]. In this paper we investigate the P-wave molecular state. Although the new experimental result suggests that the observed states are negative parity, a positive parity state may be discovered in future experiments. In particular, in the case of the hidden bottom sector, the kinetic energy is suppressed by its heavy mass, and it will be easier to be a bound than a hidden charm. Our goal in this paper is to reveal the HQS multiplet structure of the P-wave molecular state based on the LCS basis. The multiplet that can be a bound state depends on the interaction of the model. We adopt the one-pion exchange potential (OPEP) as a simple demonstration.

This paper is organized as follows. In Sect. 2 we construct the HM basis of the $\bar{P}^{(*)}\Sigma_Q^{(*)}$ states and transfer it to the LCS basis to discuss the HQS multiplet structure. The effective Lagrangians and OPEP are shown in Sect. 3. In Sect. 4 we summarize the numerical results. Finally, Sect. 5 gives a summary and discussion.

2. HQS multiplet structure of $\bar{P}^{(*)}\Sigma_Q^{(*)}$ with P-wave

In this section we consider the HQS multiplet of P-wave states. First, we construct the HM basis of the $\bar{P}^{(*)}\Sigma_Q^{(*)}$ states. The possible spin states and meson–baryon components for given J^P are shown in Table 1. Giving the $\bar{P}^{(*)}\Sigma_Q^{(*)}$ component with total spin S, we obtain the spin structure in the HM basis and the possible total angular momentum J as follows:

$$\bar{P}\Sigma_Q\left(^2P\right) = [P[[\bar{Q}q]_0[Q[d]_1]_{1/2}]_{1/2}] = \frac{1}{2}\oplus\frac{3}{2},\tag{3}$$

$$\bar{P}\Sigma_Q^*\left(^4P\right) = [P[[\bar{Q}q]_0[Q[d]_1]_{3/2}]_{3/2}] = \frac{1}{2}\oplus\frac{3}{2}\oplus\frac{5}{2},\tag{4}$$

$$\bar{P}^*\Sigma_Q\left(^2P\right) = [P[[\bar{Q}q]_1[Q[d]_1]_{1/2}]_{1/2}] = \frac{1}{2}\oplus\frac{3}{2},\tag{5}$$

$$\bar{P}^*\Sigma_Q\left(^4P\right) = [P[[\bar{Q}q]_1[Q[d]_1]_{1/2}]_{3/2}] = \frac{1}{2}\oplus\frac{3}{2}\oplus\frac{5}{2},\tag{6}$$

$$\bar{P}^*\Sigma_Q^*\left(^2P\right) = [P[[\bar{Q}q]_1[Q[d]_1]_{3/2}]_{1/2}] = \frac{1}{2}\oplus\frac{3}{2},\tag{7}$$

$$\bar{P}^* \Sigma_Q^* \left({}^4 P \right) = [P[[\bar{Q}q]_1 [Q[d]_1]_{3/2}]_{3/2}] = \frac{1}{2} \oplus \frac{3}{2} \oplus \frac{5}{2}, \tag{8}$$

$$\bar{P}^* \Sigma_Q^* \left({}^6 P \right) = [P[[\bar{Q}q]_1 [Q[d]_1]_{3/2}]_{5/2}] = \frac{3}{2} \oplus \frac{5}{2} \oplus \frac{7}{2}, \tag{9}$$

where $[L[[\bar{Q}q]_{s_1} [Q[d]_1]_{s_2}]_S]$ implies that the $\bar{P}^{(*)} \sim \bar{Q}q$ meson with spin s_1 and the $\Sigma_Q^{(*)} \sim Qd$ baryon ($d = qq$ is a light diquark) with spin s_2 are combined into a $\bar{P}^{(*)} \Sigma_Q^{(*)}$ composite state with total spin S and orbital angular momentum L. $[d]_1$ implies that the spin of the diquark is 1, because the light diquark in a $\Sigma_Q^{(*)}$ baryon has spin 1. In the HM basis it is simple to construct the possible spin states because it is just the coupling of the spins of a meson and a baryon, and the orbital angular momentum. However, the HM basis is not suitable for discussing the HQS multiplet structure. The heavy quark spin and the light-cloud spin are independently conserved in the heavy quark limit. Therefore the heavy quark spin and the other spin must be treated separately. We define the LCS basis as a suitable basis to study the structure of HQS multiplets.

In the LCS basis, the spin structures are rewritten as follows:

$$\text{(s-1): } [[\bar{Q}Q]_0 [P[q[d]_1]_1]_{1/2}]_{1/2}] = \frac{1}{2}, \tag{10}$$

$$\text{(s-2): } [[\bar{Q}Q]_0 [P[q[d]_1]_1]_{3/2}]_{1/2}] = \frac{1}{2}, \tag{11}$$

$$\text{(s-3): } [[\bar{Q}Q]_0 [P[q[d]_1]_1]_{1/2}]_{3/2}] = \frac{3}{2}, \tag{12}$$

$$\text{(s-4): } [[\bar{Q}Q]_0 [P[q[d]_1]_1]_{3/2}]_{3/2}] = \frac{3}{2}, \tag{13}$$

$$\text{(s-5): } [[\bar{Q}Q]_0 [P[q[d]_1]_1]_{3/2}]_{5/2}] = \frac{5}{2}, \tag{14}$$

$$\text{(d-1): } [[\bar{Q}Q]_1 [P[q[d]_1]_1]_{1/2}]_{1/2}] = \frac{1}{2} \oplus \frac{3}{2}, \tag{15}$$

$$\text{(d-2): } [[\bar{Q}Q]_1 [P[q[d]_1]_1]_{3/2}]_{1/2}] = \frac{1}{2} \oplus \frac{3}{2}, \tag{16}$$

$$\text{(t-1): } [[\bar{Q}Q]_1 [P[q[d]_1]_1]_{1/2}]_{3/2}] = \frac{1}{2} \oplus \frac{3}{2} \oplus \frac{5}{2}, \tag{17}$$

$$\text{(t-2): } [[\bar{Q}Q]_1 [P[q[d]_1]_1]_{3/2}]_{3/2}] = \frac{1}{2} \oplus \frac{3}{2} \oplus \frac{5}{2}, \tag{18}$$

$$\text{(t-3): } [[\bar{Q}Q]_1 [P[q[d]_1]_1]_{3/2}]_{5/2}] = \frac{3}{2} \oplus \frac{5}{2} \oplus \frac{7}{2}, \tag{19}$$

where $[\bar{Q}Q]_{s_1} [P[q[d]_1]_{s_2}]_{s_3}$ implies that a heavy quark Q and an anti-heavy quark $\bar{Q}$ are combined into a state with spin s_1 in S-wave. The spins of a light quark q and a diquark d are coupled to spin s_2 and the total spin of the combined state in P-wave is given by s_3. The right-hand sides of the equations show the possible spins of the combined pentaquark states. There are five HQS singlets (s-1 to s-5), two HQS doublets (d-1 and d-2), and three HQS triplets (t-1 to t-3). The HQS triplet does not exist in single heavy hadrons. It is a feature of the multi-heavy quark system. The basis transformation is done by

$$\psi_{J^P}^{\text{LCS}} = U_{J^P}^{-1} \psi_{J^P}^{\text{HM}}, \tag{20}$$

where U is a transformation matrix determined by the Clebsch–Gordan coefficient to reconstruct the spin structure. The detail of the basis transformation is summarized in the appendix. It is to be noted that the two heavy quarks are labeled by the same velocity v to classify the pentaquark states based on the heavy quark spin symmetry.

3.   Effective Lagrangians and potentials

In the previous section we showed that there are ten multiplets in the P-wave $\bar{P}^{(*)}\Sigma_Q^{(*)}$ molecular states. In this section we demonstrate which of the multiplets can be bound by using the one-pion exchange potential. We construct the OPEP for $\bar{P}^{(*)}\Sigma_Q^{(*)}$ molecular states based on the heavy hadron effective theory.

The $\bar{P}^{(*)}$ mesons and pion interaction Lagrangian [62–66] is given by

$$\mathcal{L}_{HH\pi} = g\mathrm{Tr}\left[\bar{H}H\gamma_\mu\gamma_5 A^\mu\right]. \tag{21}$$

The heavy meson doublet field H is

$$H = \frac{1+\slashed{v}}{2}\left[P_\mu^*\gamma^\mu + iP\gamma_5\right]. \tag{22}$$

The P and P^* are pseudoscalar meson and vector meson fields in the HQS doublet. The axial vector current for the pion is given by

$$A_\mu = \frac{i}{2}(\xi^\dagger\partial_\mu\xi - \xi\partial_\mu\xi^\dagger), \tag{23}$$

where $\xi = \exp(i\hat{\pi}/\sqrt{2}f_\pi)$. The pion decay constant is $f_\pi = 92.4\,\mathrm{MeV}$ and the pion field $\hat{\pi}$ is defined by

$$\hat{\pi} = \begin{pmatrix} \pi^0/\sqrt{2} & \pi^+ \\ \pi^- & -\pi^0/\sqrt{2} \end{pmatrix}. \tag{24}$$

The coupling constant g is determined as $|g| = 0.59$ from the decay of $D^* \to D\pi$ [69].

The $\Sigma_Q^{(*)}$ baryons and pion interaction Lagrangian [66,67] is given by

$$\mathcal{L}_{SS\pi} = \frac{3}{2}g_1 iv_\sigma\epsilon^{\mu\nu\rho\sigma}\mathrm{Tr}\left[\bar{S}_\mu A_\nu S_\rho\right]. \tag{25}$$

The superfield S_μ for Σ_Q and Σ_Q^* is represented as

$$S_\mu = \hat{\Sigma}_{Q\mu}^* - \sqrt{\frac{1}{3}}\left(\gamma_\mu + v_\mu\right)\gamma_5\hat{\Sigma}_Q. \tag{26}$$

The heavy baryon fields $\hat{\Sigma}_{Q(\mu)}^{(*)}$ are defined by

$$\hat{\Sigma}_{Q(\mu)}^{(*)} = \begin{pmatrix} \Sigma_{Q(\mu)}^{(*)++} & \frac{1}{\sqrt{2}}\Sigma_{Q(\mu)}^{(*)+} \\ \frac{1}{\sqrt{2}}\Sigma_{Q(\mu)}^{(*)+} & \Sigma_{Q(\mu)}^{(*)0} \end{pmatrix}. \tag{27}$$

Σ_Q and $\Sigma_{Q\mu}^*$ are spin 1/2 and 3/2 baryon fields in the HQS doublet. For the coupling constant g_1 we use $g_1 = (\sqrt{8}/3)g_4$ and $g_4 = 0.999$, as estimated in Ref. [67]. The coupling g_4 is determined by the decay of $\Sigma_c^* \to \Lambda_c\pi$, and its sign follows the quark model estimation.

When we construct the OPEP from effective Lagrangians we introduce a cutoff parameter Λ via the monopole type form factor

$$F(q) = \frac{\Lambda^2 - m_\pi^2}{\Lambda^2 + |\vec{q}\,|^2} \tag{28}$$

at each vertex, where m_π is the mass of the exchanging pion, and $\vec{q}$ is its momentum. We use the same cutoff for $\bar{P}^{(*)}\bar{P}^{(*)}\pi$ and $\Sigma_Q^{(*)}\Sigma_Q^{(*)}\pi$ vertices for simplicity, and fix the value of the cutoff at 800, 900, and 1000 MeV.[1] The obtained potential matrices in the HM basis are summarized in the appendix. We note that contact terms are subtracted from the potentials, because in a conventional way the OPEP has been considered at large distance [68]. Furthermore, we study the cases where the final pentaquarks carry isospin $1/2$, because P_c pentaquarks carry $I = 1/2$.

The potential matrices can also be transformed to the LCS basis by using the unitary matrix U as follows:

$$V_{1/2^+}^{\text{LCS}} = U_{1/2^+}^{-1} V_{1/2^+}^{\text{HM}} U_{1/2^+}$$

$$= \begin{pmatrix}
C & -\frac{\sqrt{2}}{2}T & 0 & 0 & 0 & 0 \\
-\frac{\sqrt{2}}{2}T & -\frac{1}{2}C + T & 0 & 0 & 0 & 0 \\
0 & 0 & C & -\frac{\sqrt{2}}{2}T & 0 & 0 \\
0 & 0 & -\frac{\sqrt{2}}{2}T & -\frac{1}{2}C + T & 0 & 0 \\
0 & 0 & 0 & 0 & C & \frac{\sqrt{5}}{10}T \\
0 & 0 & 0 & 0 & \frac{\sqrt{5}}{10}T & -\frac{1}{2}C - \frac{4}{5}T
\end{pmatrix} \frac{gg_1}{f_\pi^2}, \tag{29}$$

$$V_{3/2^+}^{\text{LCS}} = U_{3/2^+}^{-1} V_{3/2^+}^{\text{HM}} U_{3/2^+}$$

$$= \begin{pmatrix}
C & \frac{\sqrt{5}}{10}T & 0 & 0 & 0 & 0 & 0 \\
\frac{\sqrt{5}}{10}T & -\frac{1}{2}C - \frac{4}{5}T & 0 & 0 & 0 & 0 & 0 \\
0 & 0 & C & -\frac{\sqrt{2}}{2}T & 0 & 0 & 0 \\
0 & 0 & -\frac{\sqrt{2}}{2}T & -\frac{1}{2}C + T & 0 & 0 & 0 \\
0 & 0 & 0 & 0 & C & \frac{\sqrt{5}}{10}T & 0 \\
0 & 0 & 0 & 0 & \frac{\sqrt{5}}{10}T & -\frac{1}{2}C - \frac{4}{5}T & 0 \\
0 & 0 & 0 & 0 & 0 & 0 & -\frac{1}{2}C + \frac{1}{5}T
\end{pmatrix} \frac{gg_1}{f_\pi^2}, \tag{30}$$

$$V_{5/2^+}^{\text{LCS}} = U_{5/2^+}^{-1} V_{5/2^+}^{\text{HM}} U_{5/2^+}$$

$$= \begin{pmatrix}
-\frac{1}{2}C + \frac{1}{5}T & 0 & 0 & 0 \\
0 & C & \frac{\sqrt{5}}{10}T & 0 \\
0 & \frac{\sqrt{5}}{10}T & -\frac{1}{2}C - \frac{4}{5}T & 0 \\
0 & 0 & 0 & -\frac{1}{2}C + \frac{1}{5}T
\end{pmatrix} \frac{gg_1}{f_\pi^2}, \tag{31}$$

---

[1] In the previous analysis of the S-wave molecular states [61], large cutoffs, $\Lambda = 1000$ and 1500 MeV, were used, where the shallow bound state was found at the charm region with $\Lambda = 1000$ MeV. However, the tensor force producing a strong attraction was absent. In the present study, the tensor force is considered and then we may overestimate a binding energy when the large cutoff is used. Thus, we use a cutoff parameter less than or equal to 1000 MeV in the present analysis.
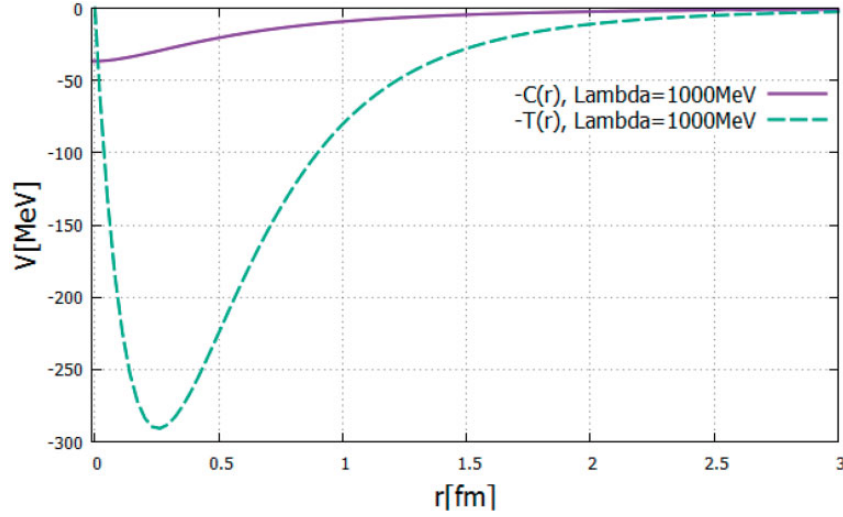
Fig. 2. Spin–spin potential C and tensor potential T with the cutoff parameter $\Lambda = 1000\,\text{MeV}$.

$$V_{7/2^+}^{\text{LCS}} = U_{7/2^+}^{-1} V_{7/2^+}^{\text{HM}} U_{7/2^+} = \frac{gg_1}{f_\pi^2}\left[-\frac{1}{2}C + \frac{1}{5}T\right], \tag{32}$$

where the functions $C(m_\pi, r, \Lambda)$ and $T(m_\pi, r, \Lambda)$ are the spin–spin potential and tensor potential, respectively. We have omitted the arguments of the potentials in the above equations. Their explicit forms are given by

$$C(m_\pi, r, \Lambda) = \frac{m_\pi^2}{4\pi}\left[\frac{e^{-m_\pi r} - e^{-\Lambda r}}{r} - \frac{\Lambda^2 - m_\pi^2}{2\Lambda}e^{-\Lambda r}\right], \tag{33}$$

$$T(m_\pi, r, \Lambda) = \frac{m_\pi^3}{4\pi}H_3(m_\pi, \Lambda, r), \tag{34}$$

$$
\begin{aligned}
H_3(m_\pi, \Lambda, r) = \frac{1}{m_\pi^3}\Bigg[&\frac{m_\pi^2 r^2 + 3m_\pi r + 3}{r^3}e^{-m_\pi r} \\
&- \frac{\Lambda^2 r^2 + 3\Lambda r + 3}{r^3}e^{-\Lambda r} \\
&- \frac{\Lambda^2 - m_\pi^2}{2r}e^{-\Lambda r} - \frac{\Lambda^3 - \Lambda m_\pi^2}{2}e^{-\Lambda r}\Bigg].
\end{aligned}
\tag{35}
$$

The typical shapes of C and T are shown in Fig. 2. This shows that the signs of C and T are negative so as to be attractive potentials.

The block matrices of the above OPEPs in the LCS basis are classified by the HQS multiplet structure. For example, the first 2×2 block in Eq. (29) is for the HQS singlet sector with total spin $1/2$. It corresponds to the first and second components in Eq. (A.6), or the (s-1) component in Eq. (10) and (s-2) in Eq. (11). Similarly, the second block in Eq. (29) corresponds to the third and fourth components in Eq. (A.6), which is for spin $(1/2, 3/2)$ doublet, and the third block in Eq. (29) corresponds to the fifth and sixth components in Eq. (A.6), which is for the spin $(1/2, 3/2, 5/2)$ triplet.

The component of the block matrix is determined by the LCS structure. For instance, the first and second blocks in Eq. (29) are identical because two $1/2$ singlets and two $(1/2, 3/2)$ doublets have the same LCS structure, $[P[q[d]_1]_{1/2}]_{1/2}$ and $[P[q[d]_1]_{3/2}]_{1/2}$, as shown in Eq. (A.6).

Table 2. Masses of relevant charmed and bottomed hadrons [69].

	$\bar{D}$	$\bar{D}^*$	B	B^*
Mass [MeV]	1867.21	2008.56	5279.48	5324.65
	Σ_c	Σ_c^*	Σ_b	Σ_b^*
Mass [MeV]	2453.54	2518.13	5813.4	5833.6

Table 3. Values of parameters to include the effect of heavy quark spin symmetry breaking in Eqs. (36)–(39).

a [GeV^2]	b [GeV^2]	c [GeV^2]	d [GeV^2]	w [GeV^3]	x [GeV^3]	y [GeV^3]	z [GeV^3]
−2.0798	−1.8685	1.9889	2.0814	2.9468	3.1677	−3.1729	−3.0629

4. Numerical result

In this section we show the binding energy obtained by solving the coupled channel Schrödinger equation under the OPEPs obtained in the previous section. The kinetic terms are written at the end of the appendix. Although they have off-diagonal terms in the LCS basis at finite mass, the kinetic terms become diagonal at the heavy quark limit. We use the Gaussian expansion method [70] to solve the Schrödinger equations. The coupling constant of the heavy meson–pion interaction determined by the decay of $D^* \to D\pi$ is $|g| = 0.59$. Following the quark-level dynamics, its sign is taken as plus. The coupling constant of the heavy baryon–pion interaction is estimated as $g_1 = 0.94$ by the quark model [67]. Therefore, the relative sign between g and g_1 in the OPEP is fixed as plus. In this paper, however, we examine both plus and minus signs to investigate the HQS multiplet structure for each case.

We include the effect of the heavy quark spin symmetry breaking by introducing the mass difference between two heavy mesons (baryons) in one HQS doublet, namely $\bar{P}$ and $\bar{P}^*$ (Σ_Q and Σ_Q^*). We parameterize the heavy hadron masses as in Ref. [61]:

$$M_{\bar{P}} = 2\mu + \frac{a}{2\mu} + \frac{w}{(2\mu)^2}, \tag{36}$$

$$M_{\bar{P}*} = 2\mu + \frac{b}{2\mu} + \frac{x}{(2\mu)^2}, \tag{37}$$

$$M_{\Sigma_Q} = 2\mu + \frac{c}{2\mu} + \frac{y}{(2\mu)^2}, \tag{38}$$

$$M_{\Sigma_Q^*} = 2\mu + \frac{d}{2\mu} + \frac{z}{(2\mu)^2}. \tag{39}$$

The mass parameter μ controls the typical mass scale. It corresponds to the averaged reduced mass of $\bar{P}\Sigma_Q$, $\bar{P}\Sigma_Q^*$, $\bar{P}^*\Sigma_Q$, and $\bar{P}^*\Sigma_Q^*$. We determine the eight parameters a, b, c, d, w, x, y, and z to reproduce the eight hadron masses shown in Table 2. The values of the eight parameters are summarized in Table 3. When $\mu = 1.102$ and 2.779 GeV the charmed and the bottomed hadron masses are reproduced, respectively. The heavy quark spin symmetry restores as the mass parameter μ increases.

We show the numerical results obtained by solving the coupled channel Schrödinger equations for each LCS structure in Figs. 3–7. The ratios of the components for some typical values of μ are summarized in Tables 4–8. This is defined from the wave function as

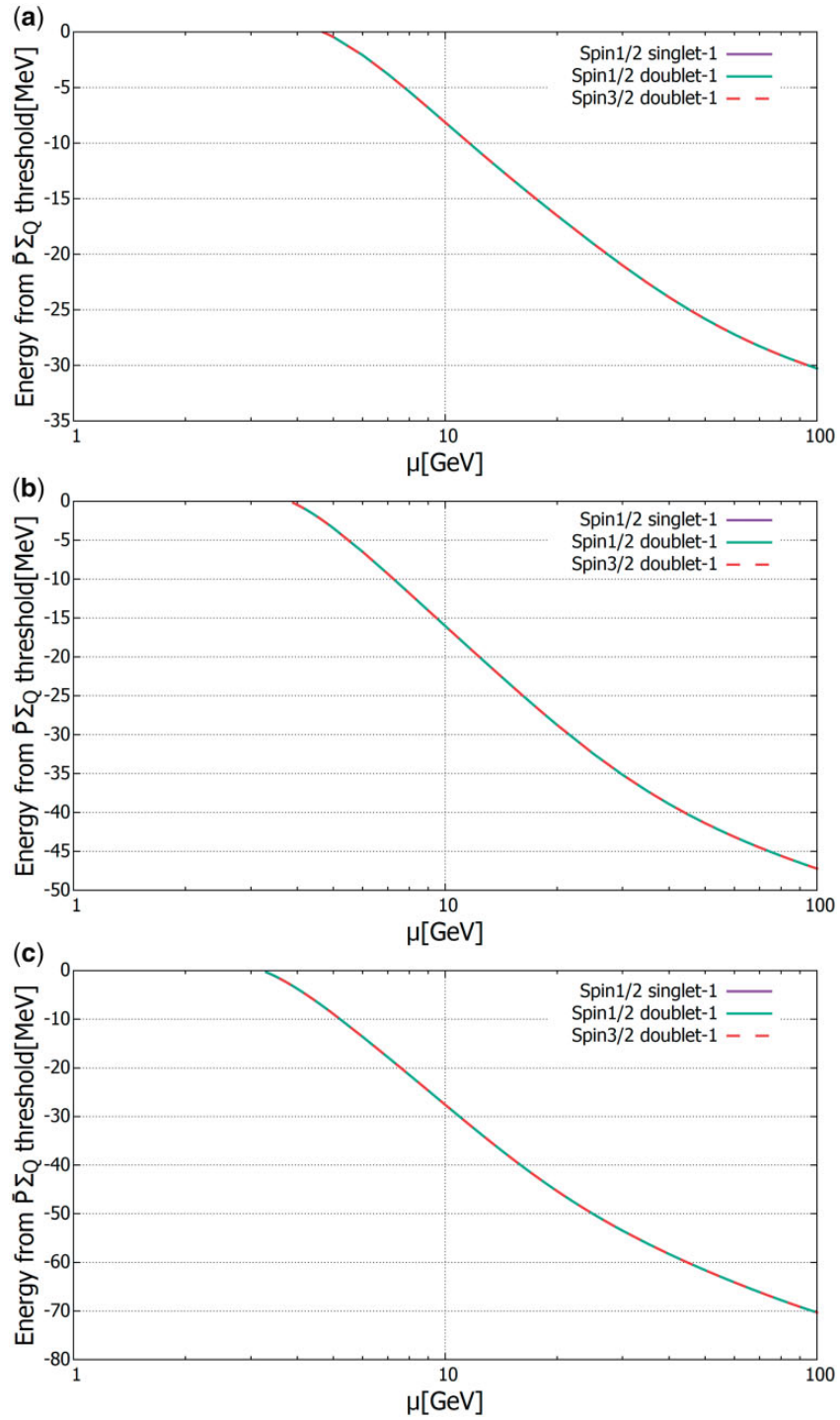$$\frac{\int dr |\psi_i|^2}{\sum_i \int dr |\psi_i|^2}. \tag{40}$$

Fig. 3. Energies for singlet-1 and doublet-1 which have the LCS structure of $[P[q[d]_1]_{1/2}]_{1/2}$ with $g = +0.59$. The cutoff parameter is (a) 800 MeV, (b) 900 MeV, and (c) 1000 MeV. The energy is measured from the threshold of $\bar{P}\Sigma_Q$. The reduced mass parameter is changed from 1 GeV to 100 GeV. The labels are defined by the main component of the wave function.

The index i denotes the component of the wave function. The labels of the bound state solutions in Figs. 3–7 are named by the main component of the wave function. For instance, the spin 1/2 HQS singlet state in Table 4 is dominated by the singlet-1 defined by Eq. (10). Therefore, the label of this state is "Spin1/2 singlet-1" in Fig. 3.
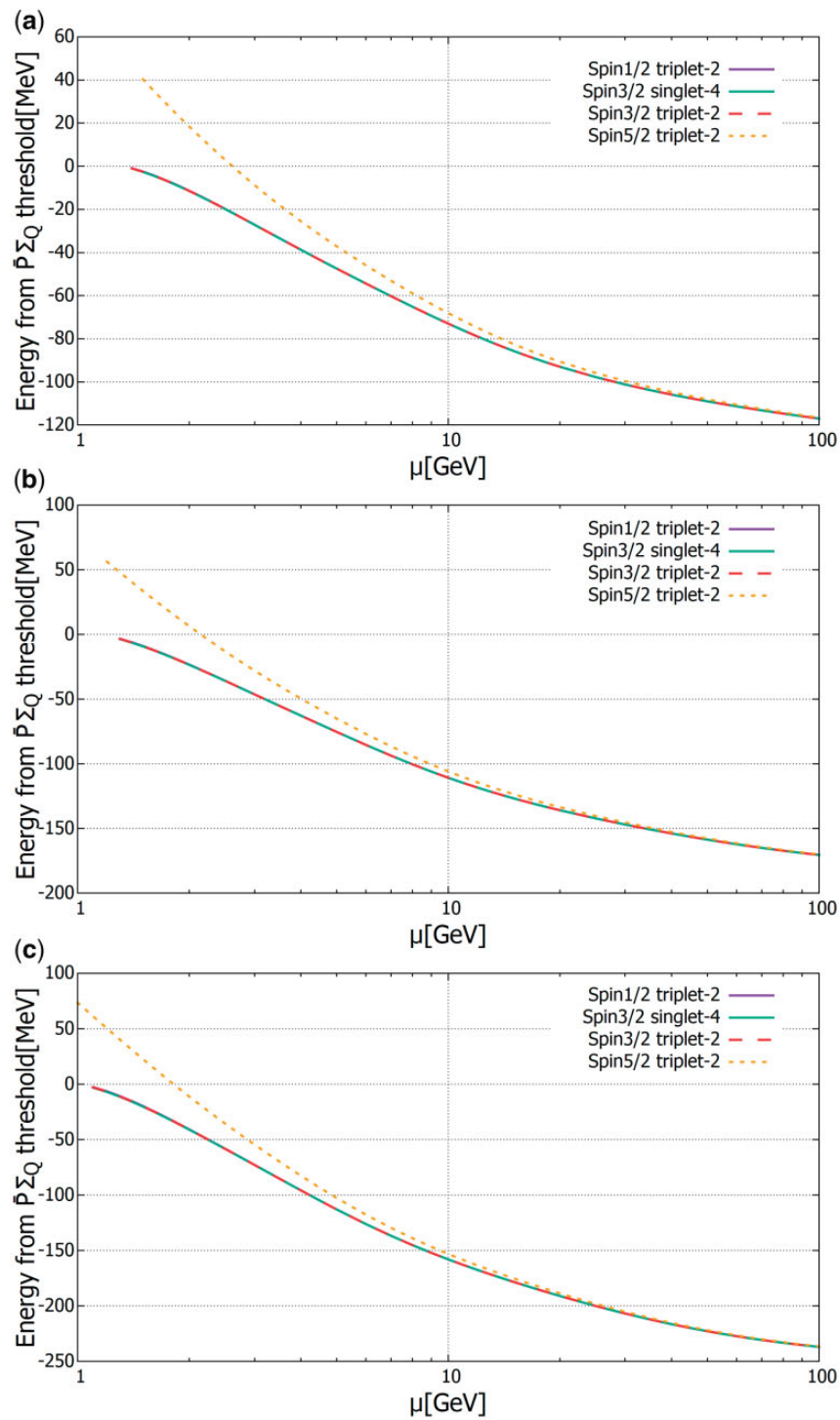
Fig. 4. Energies for singlet-4 and triplet-2 which have the LCS structure of $[P[q[d]_1]_{3/2}]_{3/2}$ with $g = +0.59$. The cutoff parameter is (a) 800 MeV, (b) 900 MeV, and (c) 1000 MeV. The energy is measured from the threshold of $\bar{P}\Sigma_Q$. The reduced mass parameter is changed from 1 GeV to 100 GeV. The labels are defined by the main component of the wave function.

When the mass parameter μ is small, the HQS doublet component is slightly mixed for the Spin1/2 singlet-1 state. This means that the HQSS breaking effect from the kinetic term is very small. On the other hand, the s-1 and s-2 are mixed for all values of μ. While we distinguish these two by the
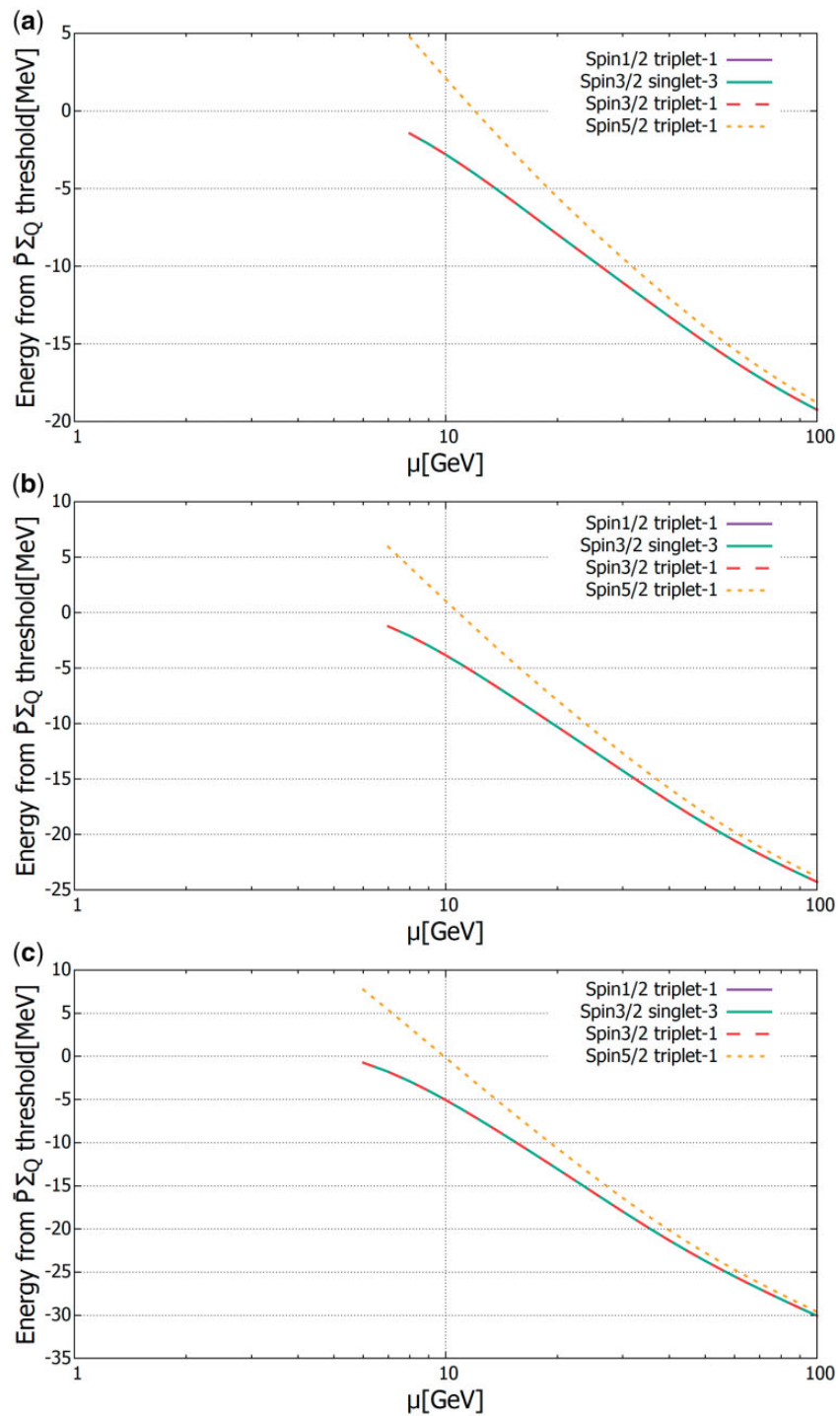
Fig. 5. Energies for singlet-3 and triplet-1 which have the LCS structure of $[P[q[d]_1]_{1/2}]_{3/2}$ with $g = -0.59$. The cutoff parameter is (a) 800 MeV, (b) 900 MeV, and (c) 1000 MeV. The energy is measured from the threshold of $\bar{P}\Sigma_Q$. The reduced mass parameter is changed from 1 GeV to 100 GeV. The labels are defined by the main component of the wave function.

difference in the internal structure of the light-cloud spin, the total spin of the light-cloud is the same. Hence they are not distinguished from the perspective of HQSS.

In the case of $g = +0.59$, the multiplets which have the light-clouds $[P[q[d]_1]_1]_{1/2}]_{1/2}$ and $[P[q[d]_1]_{3/2}]_{3/2}$ are attractive. In Fig. 3 we show the energy of $[P[q[d]_1]_1]_{1/2}]_{1/2}$, which corresponds
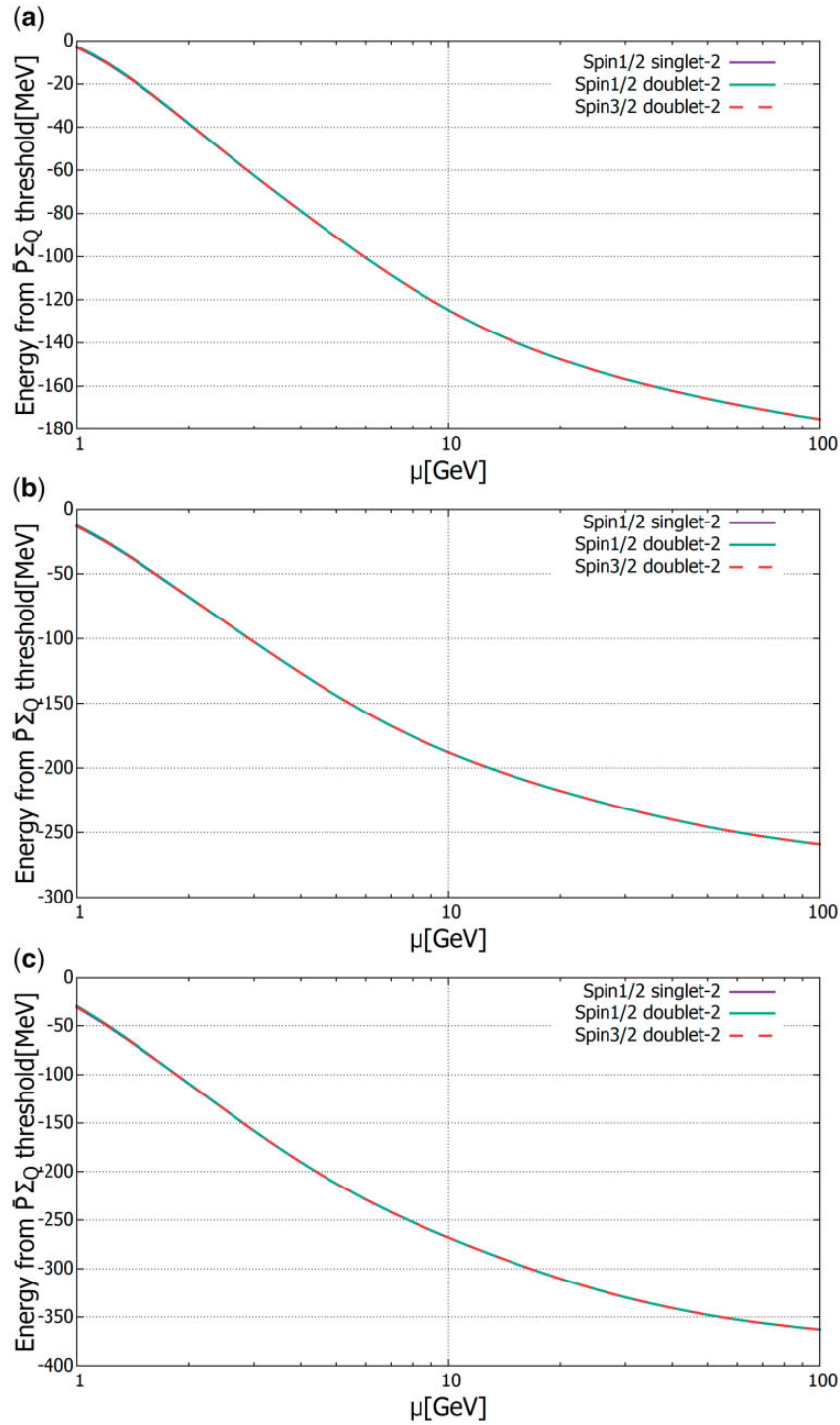
Fig. 6. Energies for singlet-2 and doublet-2 which have the LCS structure of $[P[q[d]_1]_{3/2}]_{1/2}$ with $g = -0.59$. The cutoff parameter is (a) 800 MeV, (b) 900 MeV, and (c) 1000 MeV. The energy is measured from the threshold of $\bar{P}\Sigma_Q$. The reduced mass parameter is changed from 1 GeV to 100 GeV. The labels are defined by the main component of the wave function.

to the spin 1/2 singlet (s-1) in Eq. (10) and spin (1/2, 3/2) doublet (d-1) in Eq. (15). Here, all the energies for three states are measured from the lowest threshold of $\bar{P}\Sigma_Q$. Their energies are almost degenerate for the whole range of μ. In Fig. 4 we show the energy of $[P[q[d]_1]_{3/2}]_{3/2}$, which corresponds to the spin 3/2 singlet (s-4) in Eq. (13) and spin (1/2, 3/2, 5/2) triplet (t-2) in Eq. (18). We

Fig. 7. Energies for singlet-5 and triplet-3 which have the LCS structure of $[P[q[d]_1]_{3/2}]_{5/2}$ with $g = -0.59$. The cutoff parameter is (a) 800 MeV, (b) 900 MeV, and (c) 1000 MeV. The energy is measured from the threshold of $\bar{P}\Sigma_Q$. The reduced mass parameter is changed from 1 GeV to 100 GeV. The labels are defined by the main component of the wave function.

note that the lowest threshold of the spin 1/2 and 3/2 states is $\bar{P}\Sigma_Q$, while that of the spin 5/2 state is $\bar{P}\Sigma_Q^*$. Then, the energies of the spin 5/2 state shown in Fig. 4 (and Figs. 5 and 7) are positive even if they are bound states.

Table 4. Percentage of the wave function component for singlet-1 and doublet-1 in Fig. 3 with $\Lambda = 900\,\mathrm{MeV}$. "—" implies that a bound state is not found at the parameter.

	Spin1/2 singlet-1							Spin1/2 doublet-1					
μ [GeV]	s-1	s-2	d-1	d-2	t-1	t-2		s-1	s-2	d-1	d-2	t-1	t-2
1	—	—	—	—	—	—		—	—	—	—	—	—
2	—	—	—	—	—	—		—	—	—	—	—	—
3	—	—	—	—	—	—		—	—	—	—	—	—
4	75.1	24.3	0.5	0.1	0.0	0.0		0.5	0.1	75.1	24.3	0.0	0.0
5	75.4	24.4	0.2	0.0	0.0	0.0		0.2	0.0	75.4	24.4	0.0	0.0
10	75.9	24.1	0.0	0.0	0.0	0.0		0.0	0.0	75.9	24.1	0.0	0.0
100	76.0	24.0	0.0	0.0	0.0	0.0		0.0	0.0	76.0	24.0	0.0	0.0

	Spin3/2 doublet-1						
μ [GeV]	s-1	s-2	d-1	d-2	t-1	t-2	t-3
1	—	—	—	—	—	—	
2	—	—	—	—	—	—	
3	—	—	—	—	—	—	
4	0.0	0.0	74.9	25.1	0.0	0.0	0.0
5	0.0	0.0	75.5	24.5	0.0	0.0	0.0
10	0.0	0.0	76.0	24.0	0.0	0.0	0.0
100	0.0	0.0	76.0	24.0	0.0	0.0	0.0

Table 5. Percentage of the wave function component for singlet-4 and triplet-2 in Fig. 4 with $\Lambda = 900\,\mathrm{MeV}$. "—" implies that a bound state is not found at the parameter.

	Spin1/2 triplet-2							Spin3/2 singlet-4						
μ [GeV]	s-1	s-2	d-1	d-2	t-1	t-2		s-3	s-4	d-1	d-2	t-1	t-2	t-3
1	—	—	—	—	—	—		—	—	—	—	—	—	—
2	0.0	0.0	0.0	0.0	4.8	95.2		4.7	94.0	0.0	0.0	0.0	1.3	0.0
3	0.0	0.0	0.0	0.0	4.8	95.2		4.8	95.2	0.0	0.0	0.0	0.0	0.0
4	0.0	0.0	0.0	0.0	4.8	95.2		4.8	95.2	0.0	0.0	0.0	0.0	0.0
5	0.0	0.0	0.0	0.0	4.8	95.2		4.8	95.2	0.0	0.0	0.0	0.0	0.0
10	0.0	0.0	0.0	0.0	4.8	95.2		4.8	95.2	0.0	0.0	0.0	0.0	0.0
100	0.0	0.0	0.0	0.0	4.8	95.2		4.9	95.1	0.0	0.0	0.0	0.0	0.0

	Spin3/2 triplet-2								Spin5/2 triplet-2			
μ [GeV]	s-3	s-4	d-1	d-2	t-1	t-2	t-3		s-5	t-1	t-2	t-3
1	—	—	—	—	—	—	—		—	—	—	—
2	0.0	1.3	0.0	0.0	4.7	94.0	0.0		0.0	4.7	95.3	0.0
3	0.0	0.0	0.0	0.0	4.8	95.2	0.0		0.0	4.8	95.2	0.0
4	0.0	0.0	0.0	0.0	4.8	95.2	0.0		0.0	4.8	95.2	0.0
5	0.0	0.0	0.0	0.0	4.8	95.2	0.0		0.0	4.8	95.2	0.0
10	0.0	0.0	0.0	0.0	4.8	95.2	0.0		0.0	4.8	95.2	0.0
100	0.0	0.0	0.0	0.0	4.8	95.2	0.0		0.0	4.8	95.2	0.0

Next, we show the result for $g = -0.59$. In this case, the multiplets with $[P[q[d]_1]_{1/2}]_{3/2}$, $[P[q[d]_1]_{3/2}]_{1/2}$, and $[P[q[d]_1]_{3/2}]_{5/2}$ are attractive. We show the energy of $[P[q[d]_1]_{1/2}]_{3/2}$ in Fig. 5, which corresponds to the spin 3/2 singlet (s-3) i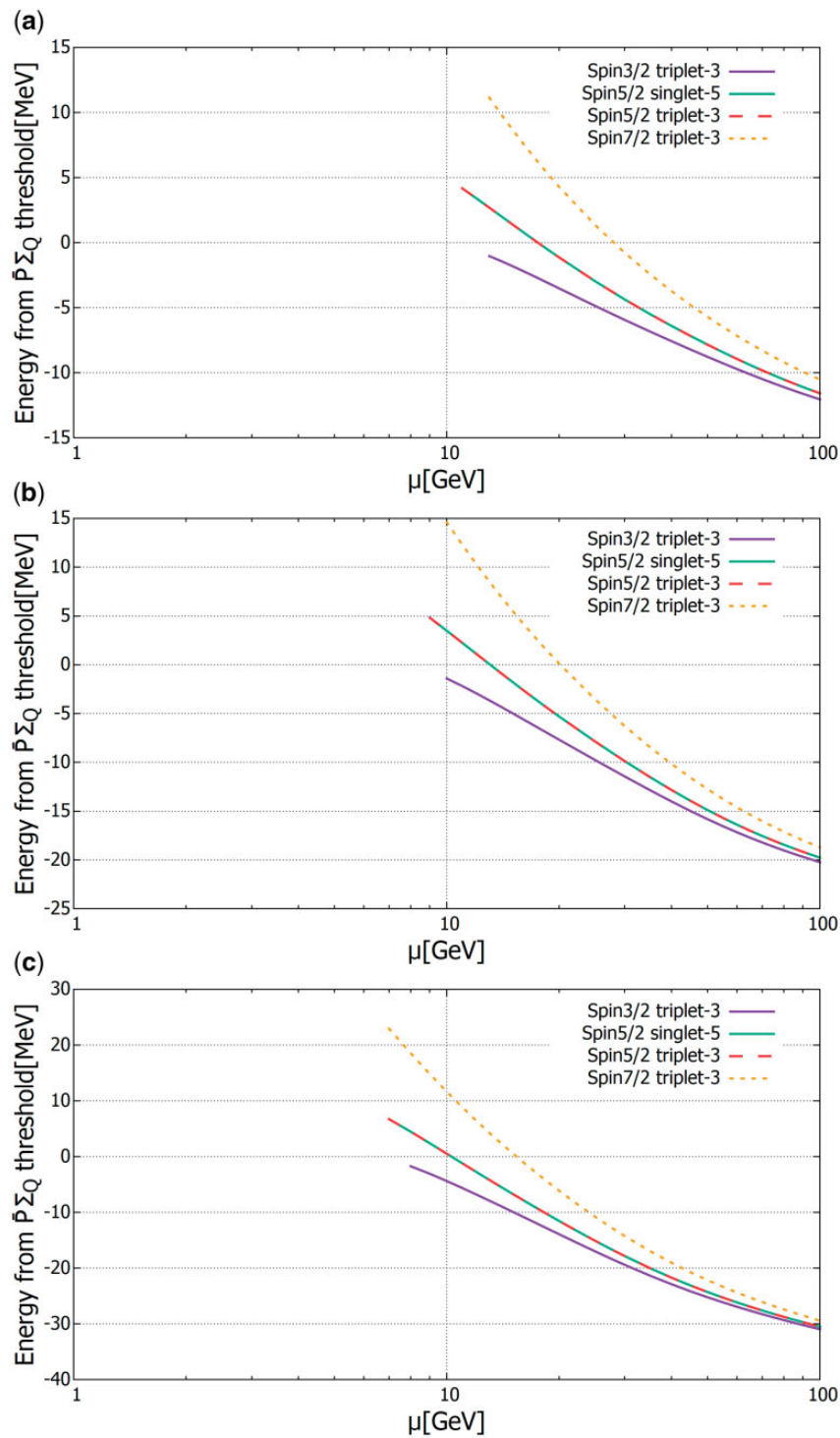n Eq. (12) and the spin (1/2, 3/2, 5/2) triplet (t-1) in Eq. (17). The lowest threshold of the spin 1/2 and 3/2 states is $\bar{P}\Sigma_Q$, while the spin 5/2

Table 6. Percentage of the wave function component for singlet-3 and triplet-1 in Fig. 5 with $\Lambda = 900$ MeV. "—" implies that a bound state is not found at the parameter.

	Spin1/2 triplet-1							Spin3/2 singlet-3						
μ [GeV]	s-1	s-2	d-1	d-2	t-1	t-2		s-3	s-4	d-1	d-2	t-1	t-2	t-3
1	—	—	—	—	—	—		—	—	—	—	—	—	—
2	—	—	—	—	—	—		—	—	—	—	—	—	—
3	—	—	—	—	—	—		—	—	—	—	—	—	—
4	—	—	—	—	—	—		—	—	—	—	—	—	—
5	—	—	—	—	—	—		—	—	—	—	—	—	—
10	0.0	0.0	0.0	0.0	95.5	4.5		95.4	4.6	0.0	0.0	0.0	0.0	0.0
100	0.0	0.0	0.0	0.0	95.1	4.9		95.1	4.9	0.0	0.0	0.0	0.0	0.0

	Spin3/2 triplet-1							Spin5/2 triplet-1			
μ [GeV]	s-3	s-4	d-1	d-2	t-1	t-2	t-3	s-5	t-1	t-2	t-3
1	—	—	—	—	—	—	—	—	—	—	—
2	—	—	—	—	—	—	—	—	—	—	—
3	—	—	—	—	—	—	—	—	—	—	—
4	—	—	—	—	—	—	—	—	—	—	—
5	—	—	—	—	—	—	—	—	—	—	—
10	0.0	0.0	0.0	0.0	95.4	4.6	0.0	0.0	95.3	4.7	0.0
100	0.0	0.0	0.0	0.0	95.2	4.8	0.0	0.0	95.3	4.7	0.0

Table 7. Percentage of the wave function component for singlet-2 and doublet-2 in Fig. 6 with $\Lambda = 900$ MeV. "—" implies that a bound state is not found at the parameter.

	Spin1/2 singlet-2							Spin1/2 doublet-2					
μ [GeV]	s-1	s-2	d-1	d-2	t-1	t-2		s-1	s-2	d-1	d-2	t-1	t-2
1	23.0	73.0	1.2	2.8	0.0	0.0		1.2	2.8	23.0	73.0	0.0	0.0
2	23.2	74.8	0.6	1.4	0.0	0.0		0.6	1.4	23.2	74.8	0.0	0.0
3	24.0	75.1	0.1	0.8	0.0	0.0		0.1	0.8	23.9	75.1	0.0	0.0
4	23.9	75.7	0.0	0.4	0.0	0.0		0.0	0.4	23.9	75.7	0.0	0.0
5	24.0	75.9	0.0	0.1	0.0	0.0		0.0	0.1	24.0	75.9	0.0	0.0
10	24.1	75.9	0.0	0.0	0.0	0.0		0.0	0.0	24.1	75.9	0.0	0.0
100	24.1	75.9	0.0	0.0	0.0	0.0		0.0	0.0	24.1	75.9	0.0	0.0

	Spin3/2 doublet-2						
μ [GeV]	s-1	s-2	d-1	d-2	t-1	t-2	t-3
1	0.0	0.0	24.3	75.7	0.0	0.0	0.0
2	0.0	0.0	24.1	75.9	0.0	0.0	0.0
3	0.0	0.0	24.0	76.0	0.0	0.0	0.0
4	0.0	0.0	23.9	76.1	0.0	0.0	0.0
5	0.0	0.0	23.9	76.1	0.0	0.0	0.0
10	0.0	0.0	24.1	75.9	0.0	0.0	0.0
100	0.0	0.0	24.1	75.9	0.0	0.0	0.0

state is $\bar{P}\Sigma_Q^*$. Next, the energy of $[P[q[d]_1]_{3/2}]_{1/2}$ is shown in Fig. 6, which corresponds to the spin 1/2 singlet (s-2) in Eq. (11) and the spin $(1/2, 3/2)$ doublet (d-2) in Eq. (16). Finally, we show the energy of $[P[q[d]_1]_{3/2}]_{5/2}$ in Fig. 7, which corresponds to the spin 5/2 singlet (s-5) in Eq. (14) and the spin $(3/2, 5/2, 7/2)$ triplet (t-3) in Eq. (19). We note that the threshold of the spin 7/2 state is

Table 8. Percentage of the wave function component for singlet-5 and triplet-3 in Fig. 7 with $\Lambda = 900$ MeV. "—" implies that a bound state is not found at the parameter.

μ [GeV]	Spin3/2 triplet-3							Spin5/2 singlet-5			
	s-3	s-4	d-1	d-2	t-1	t-2	t-3	s-5	t-1	t-2	t-3
1	—	—	—	—	—	—	—	—	—	—	—
2	—	—	—	—	—	—	—	—	—	—	—
3	—	—	—	—	—	—	—	—	—	—	—
4	—	—	—	—	—	—	—	—	—	—	—
5	—	—	—	—	—	—	—	—	—	—	—
10	0.0	0.0	0.0	0.0	0.0	0.0	100	99.8	0.0	0.0	0.2
100	0.0	0.0	0.0	0.0	0.0	0.0	100	100	0.0	0.0	0.0

μ [GeV]	Spin5/2 triplet-3				Spin7/2 triplet-3
	s-5	t-1	t-2	t-3	t-3
1	—	—	—	—	—
2	—	—	—	—	—
3	—	—	—	—	—
4	—	—	—	—	—
5	—	—	—	—	—
10	0.0	0.0	0.0	100	100
100	0.0	0.0	0.0	100	100

measured from $\bar{P}^* \Sigma_Q^*$. The difference in threshold values between $\bar{P} \Sigma_Q$ and $\bar{P} \Sigma_Q^*$ is 73.774 MeV, and between $\bar{P} \Sigma_Q$ and $\bar{P}^* \Sigma_Q^*$ is 234.63 MeV at $\mu = 1.0$ GeV.

The states which have the same LCS structure are degenerate at the heavy quark limit. However, the heavy quark spin symmetry is broken for finite quark mass, and the mass degeneracy is resolved. Although the present study includes only OPEP, the mass degeneracy should occur even using a more realistic potential model if the LCS basis is valid for the heavy meson–heavy baryon molecular state.

5.   Summary and discussions

In Sect. 2 we showed the HQS multiplet structure of molecular states made from a heavy meson and a heavy baryon in P-wave. There are five HQS singlets, two doublets, and three triplets. The OPEP is constructed by the heavy hadron effective Lagrangian, and the potential matrix is block diagonalized in the LCS basis for each HQS multiplet as shown in Sect. 3. We obtained the binding energy by solving the Schrödinger equation under OPEP in Sect. 4.

When g is positive, the spin 1/2 singlet (s-1), 3/2 singlet (s-4), the blocks of the potential for the $(1/2, 3/2)$ doublet (d-1), and the $(1/2, 3/2, 5/2)$ triplet (t-2) are attractive. The blocks for the other six multiplets, 1/2 singlet (s-2), 3/2 singlet (s-3), 5/2 singlet (s-5), $(1/2, 3/2)$ doublet (d-2), $(1/2, 3/2, 5/2)$ triplet (t-1), and $(3/2, 5/2, 7/2)$ triplet (t-3), are attractive when g is negative. The behavior of the binding energy is classified by the structure of the light-cloud spin. As mentioned in Ref. [61], OPEP depends only on the structure of the light-cloud spin since the pion exchange interaction couples the light quark spin and the orbital angular momentum. HQS multiplets with the same light-cloud structure are degenerate at the heavy quark limit. The mass degeneracy is resolved for hidden-charm/bottom pentaquarks because of the finite masses of the relevant quarks.

In Fig. 4, the singlet-4 and triplet-2 have shallow bound states at the charm region when $\Lambda = 1000$ MeV. However, there is no bound state for a smaller cutoff value, i.e. $\Lambda = 800$ and 900 MeV. The attraction by the OPEP could not be strong enough to produce a bound state of the charm region for positive g.

On the other hand, there are bound states for singlet-2 and doublet-2 even if the cutoff parameter is small in Fig. 6 when g is negative. The difference between the results for negative and positive g is caused by the role of the tensor force in the diagonal component. When g is negative, the singlet-2 and doublet-2 have strong attraction by the tensor force. For positive g, however, the overall sign of the tensor force changes, and it produces strong repulsion.

The main purpose of our present analysis is to study the HQS multiplet structure of P-wave molecular states. We have performed a simple analysis to show the diagonalization of the potential matrices and the degeneracy of the HQS multiplets as a simple demonstration. Thus, quantitative discussion of the P_c pentaquarks is difficult. For the interaction we include only the OPEP, and the short range interaction is not considered. We investigated only the bound state solution, while some of the observed P_c pentaquarks are above the $\bar{D}\Sigma_c$ threshold, which is the lowest one in this study. To address those states, we also have to study the resonant state solution. To compare with the experimental values, more precise study is needed to introduce the short range interaction and the coupling to $\bar{D}^{(*)}\Lambda_c$ and $J/\psi p$. The study of HQS multiplets with these effects is a future problem.

Moreover, P_c pentaquarks are not reproduced by the estimation of the compact five-body pentaquark [27]. Some works have discussed whether or not there is a threshold cusp due to the kinematical effect [71–74]. More theoretical efforts and experimental data are needed to reveal the nature of the P_c pentaquarks.

In this paper we determined the names of the solutions by the dominant component of the wave function, which we obtained together with the binding energy when solving the Schrödinger equation. For instance, in Figs. 8 and 9, we show the obtained wave functions of singlet-1 and triplet-2 with $J^P = 1/2^+$, for which the binding energies are shown in Figs. 3 and 4, respectively. We note that these wave functions are not normalized, therefore only the ratio of components is meaningful. In both cases, the change in the ratio of the wave functions when changing the mass parameter is very small. In the case of finite quark mass, although the different components of the HQS multiplet are mixed, the ratio is still small. This shows that the effect of the symmetry breaking by the kinetic terms is small. When the mass parameter becomes larger, the wave functions concentrate at a position where the tensor potential becomes deep. This means that, as the mass increases, the kinetic term is suppressed and the wave function is localized at the bottom of the attractive potential.

The relative motion between heavy quarks as discussed in heavy-quarkonium effective theory [75–77] is neglected in the present study, because the P-wave excitation between two heavy quarks violates the HQSS even in the leading order. Thus, the relative orbital angular momentum of two heavy quarks is always zero in the LCS basis, while the P-wave excitation occurs only in the light-cloud. Hence, a channel with P-wave quarkonium is not included in this study.

Moreover, the open heavy molecular channel cannot couple to the heavy quarkonium channel via exchange of the light meson. Very short range interaction such as heavy hadron exchange and the effect of the compact five-quark core is needed. Analysis including channels with P-wave and S-wave quarkonium is for future work.

Based on the LCS basis, the HQS singlet and the HQS doublet (or triplet) are degenerate as shown in Figs. 3–7 since they have the same LCS structure. On the other hand, their spin structure of $\bar{Q}Q$ is different: the HQS singlet is 0 and the HQS doublet (triplet) is 1. This structure makes a difference in
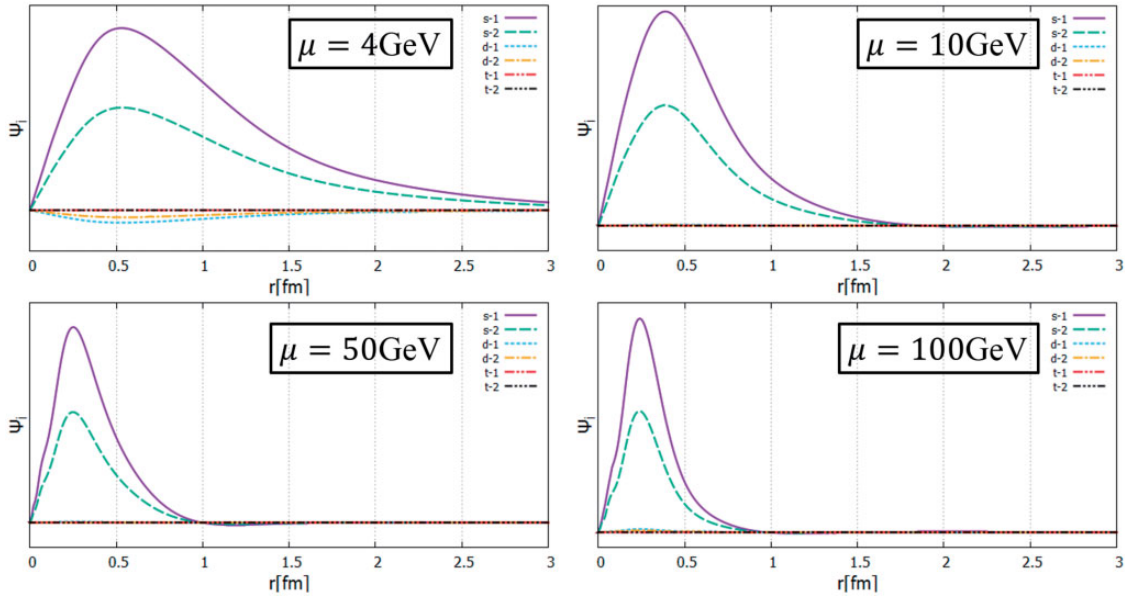
Fig. 8. Wave functions of the singlet-1 state with $J^P = 1/2^+$, $g = +0.59$, and $\Lambda = 1000$ MeV. The cases of four different mass parameters are shown.
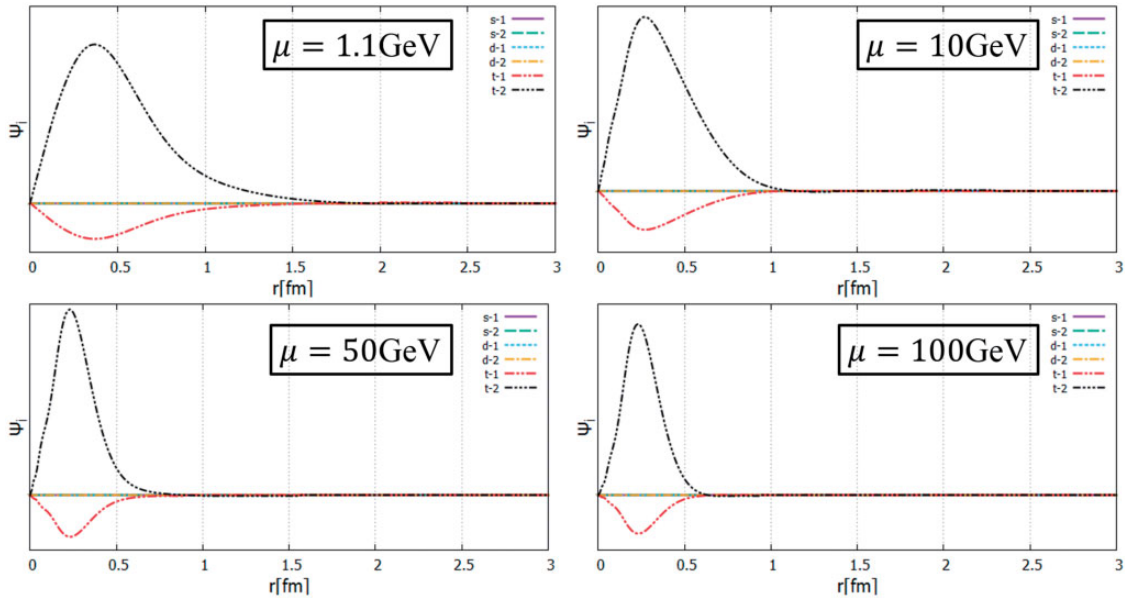

Fig. 9. Wave functions of the triplet-2 state with $J^P = 1/2^+$, $g = +0.59$, and $\Lambda = 1000$ MeV. The cases of four different mass parameters are shown.

the decay channel because the heavy spin is conserved by the HQSS. The HQS singlet can decay to spin 0 quarkonium (e.g. η_c) but cannot decay to spin 1 (e.g. J/ψ). By contrast, the HQS doublet and triplet decay to spin 1 quarkonium. Although the HQS singlet and doublet (triplet) are degenerate, they are distinguished by their decay channel if the LCS basis is valid for the heavy meson–heavy baryon molecular state.

The search for the HQS partner states of the hidden-heavy pentaquark is very important in understanding the structure of heavy hadrons. In particular, the HQSS for the hidden-bottom sector is better than for hidden-charm and easier to be bound because of its heavy mass. We expect that more diverse pentaquarks will be discovered in future experiments.

Appendix A.   Basis transformation

We show the detail of the transformation from HM basis to LCS basis. The wave function transformation is done by Eq. (20). The components of the wave functions in the HM basis for each spin state are:

$$
\psi_{1/2^+}^{\mathrm{HM}} =
\begin{pmatrix}
\bar{P}\Sigma_Q \left(^2P_{1/2}\right) \\
\bar{P}\Sigma_Q^* \left(^4P_{1/2}\right) \\
\bar{P}^*\Sigma_Q \left(^2P_{1/2}\right) \\
\bar{P}^*\Sigma_Q \left(^4P_{1/2}\right) \\
\bar{P}^*\Sigma_Q^* \left(^2P_{1/2}\right) \\
\bar{P}^*\Sigma_Q^* \left(^4P_{1/2}\right)
\end{pmatrix},
\tag{A.1}
$$

$$
\psi_{3/2^+}^{\mathrm{HM}} =
\begin{pmatrix}
\bar{P}\Sigma_Q \left(^2P_{3/2}\right) \\
\bar{P}\Sigma_Q^* \left(^4P_{3/2}\right) \\
\bar{P}^*\Sigma_Q \left(^2P_{3/2}\right) \\
\bar{P}^*\Sigma_Q \left(^4P_{3/2}\right) \\
\bar{P}^*\Sigma_Q^* \left(^2P_{3/2}\right) \\
\bar{P}^*\Sigma_Q^* \left(^4P_{3/2}\right) \\
\bar{P}^*\Sigma_Q^* \left(^6P_{3/2}\right)
\end{pmatrix},
\tag{A.2}
$$

$$
\psi_{5/2^+}^{\mathrm{HM}} =
\begin{pmatrix}
\bar{P}\Sigma_Q^* \left(^4P_{5/2}\right) \\
\bar{P}^*\Sigma_Q \left(^4P_{5/2}\right) \\
\bar{P}^*\Sigma_Q^* \left(^4P_{5/2}\right) \\
\bar{P}^*\Sigma_Q^* \left(^6P_{5/2}\right)
\end{pmatrix},
\tag{A.3}
$$

$$
\psi_{7/2^+}^{\mathrm{HM}} = \left(\ \bar{P}^*\Sigma_Q^* \left(^6P_{7/2}\right) \ \right).
\tag{A.4}
$$

The basis transformation is done by

$$\psi_{J^P}^{\mathrm{LCS}} = U_{J^P}^{-1} \psi_{J^P}^{\mathrm{HM}}. \tag{A.5}$$

The components of the wave functions in the LCS basis are:

$$\psi_{1/2^+}^{\mathrm{LCS}} = \begin{pmatrix} [[\bar{Q}Q]_0[P[q[d]_1]_1]_{1/2}]_{1/2}]_{1/2}^{\mathrm{singlet}-1} \\ [[\bar{Q}Q]_0[P[q[d]_1]_1]_{3/2}]_{1/2}]_{1/2}^{\mathrm{singlet}-2} \\ [[\bar{Q}Q]_1[P[q[d]_1]_1]_{1/2}]_{1/2}]_{1/2}^{\mathrm{doublet}-1} \\ [[\bar{Q}Q]_1[P[q[d]_1]_1]_{3/2}]_{1/2}]_{1/2}^{\mathrm{doublet}-2} \\ [[\bar{Q}Q]_1[P[q[d]_1]_1]_{1/2}]_{3/2}]_{1/2}^{\mathrm{triplet}-1} \\ [[\bar{Q}Q]_1[P[q[d]_1]_1]_{3/2}]_{3/2}]_{1/2}^{\mathrm{triplet}-2} \end{pmatrix}, \tag{A.6}$$

$$\psi_{3/2^+}^{\mathrm{LCS}} = \begin{pmatrix} [[\bar{Q}Q]_0[P[q[d]_1]_1]_{1/2}]_{3/2}]_{3/2}^{\mathrm{singlet}-3} \\ [[\bar{Q}Q]_0[P[q[d]_1]_1]_{3/2}]_{3/2}]_{3/2}^{\mathrm{singlet}-4} \\ [[\bar{Q}Q]_1[P[q[d]_1]_1]_{1/2}]_{1/2}]_{3/2}^{\mathrm{doublet}-1} \\ [[\bar{Q}Q]_1[P[q[d]_1]_1]_{3/2}]_{1/2}]_{3/2}^{\mathrm{doublet}-2} \\ [[\bar{Q}Q]_1[P[q[d]_1]_1]_{1/2}]_{3/2}]_{3/2}^{\mathrm{triplet}-1} \\ [[\bar{Q}Q]_1[P[q[d]_1]_1]_{3/2}]_{3/2}]_{3/2}^{\mathrm{triplet}-2} \\ [[\bar{Q}Q]_1[P[q[d]_1]_1]_{3/2}]_{5/2}]_{3/2}^{\mathrm{triplet}-3} \end{pmatrix}, \tag{A.7}$$

$$\psi_{5/2^+}^{\mathrm{LCS}} = \begin{pmatrix} [[\bar{Q}Q]_0[P[q[d]_1]_1]_{3/2}]_{5/2}]_{5/2}^{\mathrm{singlet}-5} \\ [[\bar{Q}Q]_1[P[q[d]_1]_1]_{1/2}]_{3/2}]_{5/2}^{\mathrm{triplet}-1} \\ [[\bar{Q}Q]_1[P[q[d]_1]_1]_{3/2}]_{3/2}]_{5/2}^{\mathrm{triplet}-2} \\ [[\bar{Q}Q]_1[P[q[d]_1]_1]_{3/2}]_{5/2}]_{5/2}^{\mathrm{triplet}-3} \end{pmatrix}, \tag{A.8}$$

$$\psi_{7/2^+}^{\mathrm{LCS}} = \begin{pmatrix} [[\bar{Q}Q]_1[P[q[d]_1]_1]_{3/2}]_{5/2}]_{7/2}^{\mathrm{triplet}-3} \end{pmatrix}. \tag{A.9}$$

The notation of the spin structure is the same as in Sect. 2. The transformation matrix U is determined by the Clebsch–Gordan coefficient to reconstruct the spin structures from the HM Basis to the LCS basis.

$$U_{1/2^+} = \begin{pmatrix} \frac{1}{2} & 0 & \frac{\sqrt{3}}{18} & \frac{2\sqrt{6}}{9} & \frac{\sqrt{6}}{9} & \frac{\sqrt{30}}{9} \\ 0 & \frac{1}{2} & \frac{2\sqrt{6}}{9} & \frac{5\sqrt{3}}{18} & -\frac{\sqrt{3}}{9} & -\frac{\sqrt{15}}{9} \\ -\frac{\sqrt{3}}{6} & 0 & -\frac{5}{18} & \frac{2\sqrt{2}}{9} & -\frac{5\sqrt{2}}{9} & \frac{\sqrt{10}}{9} \\ 0 & -\frac{\sqrt{3}}{3} & -\frac{2\sqrt{2}}{9} & \frac{5}{9} & \frac{1}{9} & -\frac{2\sqrt{5}}{9} \\ \frac{\sqrt{6}}{3} & 0 & -\frac{\sqrt{2}}{9} & -\frac{2}{9} & -\frac{4}{9} & -\frac{\sqrt{5}}{9} \\ 0 & \frac{\sqrt{15}}{6} & -\frac{2\sqrt{10}}{9} & \frac{\sqrt{5}}{18} & \frac{\sqrt{5}}{9} & -\frac{1}{9} \end{pmatrix}, \tag{A.10}$$

$$U_{3/2^+} = \begin{pmatrix} \frac{1}{2} & 0 & -\frac{\sqrt{3}}{9} & \frac{\sqrt{6}}{18} & -\frac{\sqrt{15}}{18} & \frac{2\sqrt{3}}{9} & \frac{\sqrt{2}}{2} \\ 0 & \frac{1}{2} & -\frac{\sqrt{15}}{9} & \frac{\sqrt{30}}{18} & \frac{2\sqrt{3}}{9} & \frac{11\sqrt{15}}{90} & -\frac{\sqrt{10}}{10} \\ -\frac{\sqrt{3}}{6} & 0 & \frac{5}{9} & \frac{\sqrt{2}}{18} & \frac{5\sqrt{5}}{18} & \frac{2}{9} & \frac{\sqrt{6}}{6} \\ 0 & -\frac{\sqrt{3}}{3} & \frac{\sqrt{5}}{9} & \frac{\sqrt{10}}{9} & -\frac{2}{9} & \frac{11\sqrt{5}}{45} & -\frac{\sqrt{30}}{15} \\ \frac{\sqrt{6}}{3} & 0 & \frac{2\sqrt{2}}{9} & -\frac{1}{18} & \frac{\sqrt{10}}{9} & -\frac{\sqrt{2}}{9} & -\frac{\sqrt{3}}{6} \\ 0 & \frac{\sqrt{15}}{6} & \frac{5}{9} & \frac{\sqrt{2}}{18} & -\frac{2\sqrt{5}}{9} & \frac{11}{90} & -\frac{\sqrt{6}}{30} \\ 0 & 0 & 0 & \frac{\sqrt{3}}{2} & 0 & -\frac{\sqrt{6}}{5} & \frac{1}{10} \end{pmatrix}, \tag{A.11}$$

$$U_{5/2^+} = \begin{pmatrix} \frac{1}{2} & -\frac{\sqrt{3}}{3} & \frac{\sqrt{15}}{15} & \frac{\sqrt{35}}{10} \\ -\frac{\sqrt{3}}{3} & \frac{1}{3} & \frac{2\sqrt{5}}{15} & \frac{\sqrt{105}}{15} \\ \frac{\sqrt{15}}{6} & \frac{\sqrt{5}}{3} & \frac{1}{15} & \frac{\sqrt{21}}{30} \\ 0 & 0 & \frac{\sqrt{21}}{5} & -\frac{2}{5} \end{pmatrix}, \tag{A.12}$$

$$U_{7/2^+} = 1. \tag{A.13}$$

In Sect. 3 we construct the one-pion exchange potential from the heavy hadron effective Lagrangians in the HM basis. The details of the OPEP matrix in the HM basis are as follows:

$V_{1/2^+}^{\mathrm{HM}}$

$$= \begin{pmatrix} 0 & 0 & -\frac{\sqrt{3}}{3}C & \frac{\sqrt{6}}{3}T & \frac{\sqrt{6}}{6}C & \frac{\sqrt{30}}{30}T \\ 0 & 0 & \frac{\sqrt{6}}{6}T & -\frac{\sqrt{3}}{6}C - \frac{\sqrt{3}}{6}T & -\frac{\sqrt{3}}{6}T & -\frac{\sqrt{15}}{6}C + \frac{2\sqrt{15}}{15}T \\ -\frac{\sqrt{3}}{3}C & \frac{\sqrt{6}}{6}T & \frac{2}{3}C & \frac{\sqrt{2}}{3}T & \frac{\sqrt{2}}{6}C & \frac{2\sqrt{10}}{15}T \\ \frac{\sqrt{6}}{3}T & -\frac{\sqrt{3}}{6}C - \frac{\sqrt{3}}{6}T & \frac{\sqrt{2}}{3}T & -\frac{1}{3}C + \frac{2}{3}T & \frac{1}{6}T & \frac{\sqrt{5}}{6}C - \frac{\sqrt{5}}{30}T \\ \frac{\sqrt{6}}{6}C & -\frac{\sqrt{3}}{6}T & \frac{\sqrt{2}}{6}C & \frac{1}{6}T & \frac{5}{6}C & -\frac{7\sqrt{5}}{30}T \\ \frac{\sqrt{30}}{30}T & -\frac{\sqrt{15}}{6}C + \frac{2\sqrt{15}}{15}T & \frac{2\sqrt{10}}{15}T & \frac{\sqrt{5}}{6}C - \frac{\sqrt{5}}{30}T & -\frac{7\sqrt{5}}{30}T & \frac{1}{3}C + \frac{8}{15}T \end{pmatrix} \frac{gg_1}{f_\pi^2}, \tag{A.14}$$

$V_{3/2^+}^{\mathrm{HM}}$

$$= \begin{pmatrix} 0 & 0 & -\frac{\sqrt{3}}{3}C & -\frac{\sqrt{15}}{15}T & \frac{\sqrt{6}}{6}C & -\frac{\sqrt{3}}{30}T & \frac{3\sqrt{2}}{10}T \\ 0 & 0 & -\frac{\sqrt{15}}{30}T & -\frac{\sqrt{3}}{6}C + \frac{2\sqrt{3}}{15}T & \frac{\sqrt{30}}{60}T & -\frac{\sqrt{15}}{6}C - \frac{8\sqrt{15}}{75}T & \frac{21\sqrt{10}}{100}T \\ -\frac{\sqrt{3}}{3}C & -\frac{\sqrt{15}}{30}T & \frac{2}{3}C & -\frac{\sqrt{5}}{15}T & \frac{\sqrt{2}}{6}C & -\frac{2}{15}T & -\frac{\sqrt{6}}{10}T \\ -\frac{\sqrt{15}}{15}T & -\frac{\sqrt{3}}{6}C + \frac{2\sqrt{3}}{15}T & -\frac{\sqrt{5}}{15}T & -\frac{1}{3}C - \frac{8}{15}T & -\frac{\sqrt{10}}{60}T & \frac{\sqrt{5}}{6}C + \frac{2\sqrt{5}}{75}T & \frac{7\sqrt{30}}{100}T \\ \frac{\sqrt{6}}{6}C & \frac{\sqrt{30}}{60}T & \frac{\sqrt{2}}{6}C & -\frac{\sqrt{10}}{60}T & \frac{5}{6}C & \frac{7\sqrt{2}}{60}T & -\frac{\sqrt{3}}{5}T \\ -\frac{\sqrt{3}}{30}T & -\frac{\sqrt{15}}{6}C - \frac{8\sqrt{15}}{75}T & -\frac{2}{15}T & \frac{\sqrt{5}}{6}C + \frac{2\sqrt{5}}{75}T & \frac{7\sqrt{2}}{60}T & \frac{1}{3}C - \frac{32}{75}T & -\frac{7\sqrt{6}}{100}T \\ \frac{3\sqrt{2}}{10}T & \frac{21\sqrt{10}}{100}T & -\frac{\sqrt{6}}{10}T & \frac{7\sqrt{30}}{100}T & -\frac{\sqrt{3}}{5}T & -\frac{7\sqrt{6}}{100}T & -\frac{1}{2}C + \frac{14}{25}T \end{pmatrix} \frac{gg_1}{f_\pi^2}, \tag{A.15}$$

$$
V_{5/2^+}^{\mathrm{HM}} = \begin{pmatrix}
0 & -\frac{\sqrt{3}}{6}C - \frac{\sqrt{3}}{30}T & -\frac{\sqrt{15}}{6}C + \frac{2\sqrt{15}}{75}T & -\frac{3\sqrt{35}}{50}T \\
-\frac{\sqrt{3}}{6}C - \frac{\sqrt{3}}{30}T & -\frac{1}{3}C + \frac{2}{15}T & \frac{\sqrt{5}}{6}C - \frac{\sqrt{5}}{150}T & -\frac{\sqrt{105}}{50}T \\
-\frac{\sqrt{15}}{6}C + \frac{2\sqrt{15}}{75}T & \frac{\sqrt{5}}{6}C - \frac{\sqrt{5}}{150}T & \frac{1}{3}C + \frac{8}{75}T & \frac{\sqrt{21}}{50}T \\
-\frac{3\sqrt{35}}{50}T & -\frac{\sqrt{105}}{50}T & \frac{\sqrt{21}}{50}T & -\frac{1}{2}C - \frac{16}{25}T
\end{pmatrix} \frac{gg_1}{f_\pi^2},
$$

(A.16)

$$
V_{7/2^+}^{\mathrm{HM}} = \frac{gg_1}{f_\pi^2}\left[-\frac{1}{2}C + \frac{1}{5}T \right].
$$

(A.17)

The definition of the spin–spin potential C and tensor potential T are written in Sect. 3. The tranformation of the potential matrix from HM basis to LCS basis is done by

$$
V_{J^P}^{\mathrm{LCS}} = U_{J^P}^{-1} V_{J^P}^{\mathrm{HM}} U_{J^P}.
$$

(A.18)

The potential matrices in the LCS basis are written in Sect. 3.

The kinetic term is defined by

$$
K_i^L = -\frac{1}{2\mu_i}\left(\frac{\partial^2}{\partial r^2} + \frac{2}{r}\frac{\partial}{\partial r} - \frac{L(L+1)}{r^2} \right),
$$

(A.19)

where i is the channel index, L is the orbital angular momentum, and μ_i is the reduced mass of channel i. The kinetic term matrices for each J^P in the HM basis are as follows:

$$
K_{1/2^+}^{\mathrm{HM}} = \mathrm{diag}\left[K_{\bar{P}\Sigma_Q}^1, K_{\bar{P}\Sigma_Q^*}^1, K_{\bar{P}^*\Sigma_Q}^1, K_{\bar{P}^*\Sigma_Q}^1, K_{\bar{P}^*\Sigma_Q^*}^1, K_{\bar{P}^*\Sigma_Q^*}^1 \right],
$$

(A.20)

$$
K_{3/2^+}^{\mathrm{HM}} = \mathrm{diag}\left[K_{\bar{P}\Sigma_Q}^1, K_{\bar{P}\Sigma_Q^*}^1, K_{\bar{P}^*\Sigma_Q}^1, K_{\bar{P}^*\Sigma_Q}^1, K_{\bar{P}^*\Sigma_Q^*}^1, K_{\bar{P}^*\Sigma_Q^*}^1, K_{\bar{P}^*\Sigma_Q^*}^1 \right],
$$

(A.21)

$$
K_{5/2^+}^{\mathrm{HM}} = \mathrm{diag}\left[K_{\bar{P}\Sigma_Q^*}^1, K_{\bar{P}^*\Sigma_Q}^1, K_{\bar{P}^*\Sigma_Q^*}^1, K_{\bar{P}^*\Sigma_Q^*}^1 \right],
$$

(A.22)

$$
K_{7/2^+}^{\mathrm{HM}} = K_{\bar{P}^*\Sigma_Q^*}^1.
$$

(A.23)

The transformation to the LCS basis is done by

$$
K_{J^P}^{\mathrm{LCS}} = U_{J^P}^{-1} K_{J^P}^{\mathrm{HM}} U_{J^P}.
$$

(A.24)

$K_{J^P}^{\mathrm{LCS}}$ has off-diagonal components at finite heavy quark mass. This is caused by the breaking effect of HQSS. The mixing of the different multiplets at small μ in Tables 4–8 comes from the HQSS breaking in kinetic terms. At the heavy quark limit, however, the kinetic terms in the LCS basis become diagonal.

References

[1] R. Aaij et al. [LHCb Collaboration], Phys. Rev. Lett. **115**, 072001 (2015).
[2] R. Aaij et al. [LHCb Collaboration], Phys. Rev. Lett. **117**, 082002 (2016).
[3] R. Aaij et al. [LHCb Collaboration], Phys. Rev. Lett. **117**, 082003 (2016); **117**, 109902 (2016); **118**, 119901 (2017) [errata].
[4] J.-J. Wu, R. Molina, E. Oset, and B. S. Zou, Phys. Rev. Lett. **105**, 232001 (2010).
[5] Z. C. Yang, Z. F. Sun, J. He, X. Liu, and S. L. Zhu, Chin. Phys. C **36**, 6 (2012).
[6] W. L. Wang, F. Huang, Z. Y. Zhang, and B. S. Zou, Phys. Rev. C **84**, 015203 (2011).
[7] J.-J. Wu, T.-S. H. Lee, and B. S. Zou, Phys. Rev. C **85**, 044002 (2012).
[8] R. Chen, X. Liu, X.-Q. Li, and S.-L. Zhu, Phys. Rev. Lett. **115**, 132002 (2015).

[9]   J. He, Phys. Lett. B **753**, 547 (2016).
[10] H.-X. Chen, W. Chen, X. Liu, T. G. Steele, and S.-L. Zhu, Phys. Rev. Lett. **115**, 172001 (2015).
[11] H. Huang, C. Deng, J. Ping, and F. Wang, Eur. Phys. J. C **76**, 624 (2016).
[12] L. Roca, J. Nieves, and E. Oset, Phys. Rev. D **92**, 094003 (2015).
[13] U.-G. Meißner and J. A. Oller, Phys. Lett. B **751**, 59 (2015).
[14] C. W. Xiao and U.-G. Meißner, Phys. Rev. D **92**, 114002 (2015).
[15] T. J. Burns, Eur. Phys. J. A **51**, 152 (2015).
[16] D. E. Kahana and S. H. Kahana, arXiv:1512.01902 [hep-ph] [Search INSPIRE].
[17] H.-X. Chen, E.-L. Cui, W. Chen, X. Liu, T. G. Steele, and S.-L. Zhu, Eur. Phys. J. C **76**, 572 (2016).
[18] C.-W. Shen, F.-K. Guo, J.-J. Xie, and B.-S. Zou, Nucl. Phys. A **954**, 393 (2016).
[19] Y. Shimizu, D. Suenaga, and M. Harada, Phys. Rev. D **93**, 114003 (2016).
[20] Y. Yamaguchi and E. Santopinto, Phys. Rev. D **96**, 014018 (2017).
[21] J. He, Phys. Rev. D **95**, 074004 (2017).
[22] P. G. Ortega, D. R. Entem, and F. Fernández, Phys. Lett. B **764**, 207 (2017).
[23] K. Azizi, Y. Sarac, and H. Sundu, Phys. Rev. D **95**, 094016 (2017).
[24] L.-S. Geng, J.-X. Lu, and M. P. Valderrama, Phys. Rev. D **97**, 094036 (2018) [arXiv:1704.06123 [hep-ph]] [Search INSPIRE].
[25] E. Santopinto and A. Giachino, Phys. Rev. D **96**, 014014 (2017).
[26] J. Wu, Y.-R. Liu, K. Chen, X. Liu, and S.-L. Zhu, Phys. Rev. D **95**, 034002 (2017).
[27] E. Hiyama, A. Hosaka, M. Oka, and J.-M. Richard, Phys. Rev. C **98**, 045208 (2018).
[28] L. Maiani, A. D. Polosa, and V. Riquer, Phys. Lett. B **749**, 289 (2015).
[29] R. F. Lebed, Phys. Lett. B **749**, 454 (2015).
[30] G.-N. Li, X.-G. He, and M. He, J. High Energy Phys. **1512**, 128 (2015).
[31] Z.-G. Wang, Eur. Phys. J. C **76**, 70 (2016).
[32] R. Zhu and C.-F. Qiao, Phys. Lett. B **756**, 259 (2016).
[33] S. Takeuchi and M. Takizawa, Phys. Lett. B **764**, 254 (2017).
[34] V. Kubarovsky and M. B. Voloshin, Phys. Rev. D **92**, 031502(R) (2015).
[35] M. I. Eides, V. Yu. Petrov, and M. V. Polyakov, Eur. Phys. J. C **78**, 36 (2018).
[36] N. N. Scoccola, D. O. Riska, and M. Rho, Phys. Rev. D **92**, 051501(R) (2015).
[37] Y. Liu and I. Zahed, Phys. Rev. D **96**, 056027 (2017).
[38] Y. Yamaguchi, A. Giachino, A. Hosaka, E. Santopinto, S. Takeuchi, and M. Takizawa, Phys. Rev. D **96**, 114031 (2017).
[39] H.-X. Chen, W. Chen, X. Liu, and S.-L. Zhu, Phys. Rept. **639**, 1 (2016).
[40] A. Ali, J. S. Lange, and S. Stone, Prog. Part. Nucl. Phys. **97**, 123 (2017).
[41] F.-K. Guo, C. Hanhart, U.-G. Meißner, Q. Wang, Q. Zhao, and B.-S. Zou, Rev. Mod. Phys. **90**, 015004 (2018).
[42] R. Aaij et al. [LHCb Collaboration], Phys. Rev. Lett. **122**, 222001 (2019).
[43] R. Chen, Z.-F. Sun, X. Liu, and S.-L. Zhu, Phys. Rev. D **100**, 011502(R) (2019).
[44] M.-Z. Liu, Y.-W. Pan, F.-Z. Peng, M. Sánchez, L.-S. Geng, A. Hosaka, and M. Pavon Valderrama, Phys. Rev. Lett. **122**, 242001 (2019).
[45] J. He, Eur. Phys. J. C **79**, 393 (2019).
[46] Y. Shimizu, Y. Yamaguchi, and M. Harada, arXiv:1904.00587 [hep-ph] [Search INSPIRE].
[47] Z.-H. Guo and J. A. Oller, Phys. Lett. B **793**, 144 (2019).
[48] C. W. Xiao, J. Nieves, and E. Oset, Phys. Rev. D **100**, 014021 (2019).
[49] L. Meng, B. Wang, G.-J. Wang, and S.-L. Zhu, Phys. Rev. D **100**, 014031 (2019).
[50] C. W. Xiao, J. Nieves, and E. Oset, Phys. Rev. D **799**, 135051 (2019) [arXiv:1906.09010 [hep-ph]] [Search INSPIRE].
[51] S. Sakai, H.-J. Jing, and F.-K. Guo, Phys. Rev. D **100**, 074007 (2019) [arXiv:1907.03414 [hep-ph]] [Search INSPIRE].
[52] Y. Yamaguchi, H. Garcia-Tecocoatzi, A. Giachino, A. Hosaka, E. Santopinto, S. Takeuchi, and M. Takizawa, arXiv:1907.04684 [hep-ph] [Search INSPIRE].
[53] N. Isgur and M. B. Wise, Phys. Lett. B **232**, 113 (1989).
[54] N. Isgur and M. B. Wise, Phys. Lett. B **237**, 527 (1990).
[55] N. Isgur and M. B. Wise, Phys. Rev. Lett. **66**, 1130 (1991).
[56] M. Neubert, Phys. Rept. **245**, 259 (1994).
[57] A. V. Manohar and M. B. Wise, *Heavy Quark Physics* (Cambridge University Press, Cambridge, 2000).

[58] S. Yasui, K. Sudoh, Y. Yamaguchi, S. Ohkoda, A. Hosaka, and T. Hyodo, Phys. Lett. B **727**, 185 (2013).
[59] Y. Yamaguchi, S. Ohkoda, A. Hosaka, T. Hyodo, and S. Yasui, Phys. Rev. D **91**, 034034 (2015).
[60] A. Hosaka, T. Hyodo, K. Sudoh, Y. Yamaguchi, and S. Yasui, Prog. Part. Nucl. Phys. **96**, 88 (2017).
[61] Y. Shimizu, Y. Yamaguchi, and M. Harada, Phys. Rev. D **98**, 014021 (2018).
[62] A. F. Falk, Nucl. Phys. B **378**, 79 (1992).
[63] M. B. Wise, Phys. Rev. D **45**, R2188(R) (1992).
[64] P. Cho, Phys. Lett. B **285**, 145 (1992).
[65] A. F. Falk and M. Luke, Phys. Lett. B **292**, 119 (1992).
[66] T.-M. Yan, H.-Y. Cheng, C.-Y. Cheung, G.-L. Lin, Y.-C. Lin, and H.-L. Yu, Phys. Rev. D **46**, 1148 (1992); **55**, 5851 (1997) [erratum].
[67] Y.-R. Liu and M. Oka, Phys. Rev. D **85**, 014015 (2012).
[68] A. Bohr and B. R. Mottelson, *Nuclear Structure*, (W. A. Benjamin, Inc., New York, 1969), Vol. 1.
[69] M. Tanabashi et al. [Particle Data Group], Phys. Rev. D **98**, 030001 (2018).
[70] E. Hiyama, Y. Kino, and M. Kamimura, Prog. Part. Nucl. Phys. **51**, 223 (2003).
[71] F.-K. Guo, U.-G. Meißner, W. Wang, and Z. Yang, Phys. Rev. D **92**, 071502(R) (2015).
[72] X.-H. Liu, Q. Wang, and Q. Zhao, Phys. Lett. B **757**, 231 (2016).
[73] F.-K. Guo, U.-G. Meißner, J. Nieves, and Z. Yang, Eur. Phys. J. A **52**, 318 (2016).
[74] M. Bayar, F. Aceti, F.-K. Guo, and E. Oset, Phys. Rev. D **94**, 074039 (2016).
[75] T. Mannel and G. A. Schuler, Phys. Lett. B **349**, 181 (1995).
[76] T. Mannel and G. A. Schuler, Z. Phys. C **67**, 159 (1995).
[77] R. Casalbuoni, A. Deandrea, N. Di Bartolomeo, R. Gatto, F. Feruglio, and G. Nardulli, Phys. Rept. **281**, 145 (1997).